INDENV 1 (2024) 100048

Contents lists available at ScienceDirect

Indoor Environments

journal homepage: www.sciencedirect.com/journal/indoor-environments

# Personalized low-cost thermal comfort monitoring using IoT technologies

Carlos Chillón Geck [a,*], Hayder Alsaad [b], Conrad Voelker [b], Kay Smarsly [a]

[a] Institute of Digital and Autonomous Construction, Hamburg University of Technology, Blohmstraße 15, Hamburg 21079, Germany
[b] Chair of Building Physics, Bauhaus-Universität Weimar, Coudraystrasse 11a, Weimar 99423, Germany

ARTICLE INFO

*Keywords:*
Thermal comfort
Internet of Things (IoT)
Smart buildings
Smart home
Wireless sensor networks
Intelligent sensor nodes
Building automation

ABSTRACT

Thermal comfort plays an essential role in the well-being and productivity of occupants. Typically, thermal comfort is assessed either through surveys completed by building occupants or through sensor data that is analyzed using thermal comfort models. Automating comfort surveys and data collection processes reduce the risk of information loss, providing more accurate and personalized thermal comfort assessments over longer periods of time. To this end, this paper presents the design and implementation of a thermal comfort monitoring system consisting of low-cost hardware components and using IoT technologies. The system consists of intelligent wireless sensor nodes that collect and process environmental data, a portable main station that integrates and stores data, and a digital survey that provides feedback from building occupants. To ensure accuracy, the low-cost hardware components of the intelligent sensor nodes are calibrated in a climate chamber, using high-precision sensors for reference. After calibration, the system is deployed in a field test where several intelligent sensor nodes collect environmental data in an office, while occupants complete the digital thermal comfort survey. In addition, thermal comfort indexes are computed by the intelligent sensor nodes and compared with the feedback of each building occupant. The results indicate that the low-cost thermal comfort monitoring system successfully collects and integrates thermal comfort data from the intelligent sensor nodes and the digital survey, being able to create personalized thermal comfort profiles. In future work, the system can be used in large-scale thermal comfort surveys, to develop personalized thermal comfort models and to control personalized comfort systems.

## 1. Introduction

As a consequence of the COVID-19 pandemic, people are relying on higher air changes, e.g., by periodic natural ventilation opening windows [1]. On the one hand, the intensified ventilation increases protection against infection, but on the other hand, it also means higher energy consumption due to building operations [2], with the risk of thermal discomfort due to draft or low indoor temperatures [3]. Thus, in recent years, there have been significant constraints regarding thermal comfort despite of its substantial influence on health and productivity of occupants.

Thermal discomfort, the opposite of thermal comfort, experienced over extended periods of time may lead to the appearance of adverse health symptoms [4] or health disorders, such as sick building syndrome or building-related illness [5]. Moreover, extreme events, such as heat waves or sub-zero temperatures, are the causes of a large number of annual deaths, particularly elderly, children, and people suffering from energy poverty [6]. In addition to health, productivity related to office tasks, such as typing or logical thinking, can also be affected by thermal discomfort [7].

Traditionally, thermal comfort has been investigated from a physiological perspective, aiming to develop comfort indexes using heat-balance models and laboratory environments [8]. One of these heat-balance models is the predicted mean vote (PMV) index measuring thermal comfort in buildings. The PMV assesses thermal comfort by forecasting thermal comfort of occupants feeling based on six key factors, environmental conditions, encompassing (1) indoor air temperature ($t_a$), (2) relative humidity ($RH$), (3) air velocity ($v_a$); and (4) mean radiant temperature ($MRT$), and personal factors, including the (5) metabolic rate (met) and the (6) clothing insulation ($I_{cl}$) of the clothing ensembles worn by the occupants. The PMV index was developed by Fanger [9] in the 1970s and has since become a widely accepted standard for predicting thermal comfort. The predicted percentage of dissatisfied (PPD), determined from the PMV index, gives an estimation of the percentage of people that feel uncomfortable under certain thermal conditions. However, the PMV and the PPD indexes calculate the

* Corresponding author.
*E-mail address:* carlos.chillon.geck@tuhh.de (C.C. Geck).

https://doi.org/10.1016/j.indenv.2024.100048
Received 26 January 2024; Received in revised form 20 June 2024; Accepted 16 September 2024
Available online 17 September 2024

average feeling of comfort of a group of people, but does not consider every individual separately. Thus, research in the field of thermal comfort has shifted towards personalized thermal comfort, which can only be achieved by granting building occupants control over their individual thermal environments [10].

A widely used approach to obtain personalized thermal comfort is implementing monitoring systems that assess thermal comfort at the macroenvironment near the users [11]. Monitoring systems based on Internet of Things (IoT) technologies have become cost-efficient and reliable [12], particularly in smart home and smart building applications [13]. Due to the growing availability and quality of sensors and microcontrollers, low-cost sensor nodes have been used to continuously measure environmental parameters [14]. In [15], the overall cost of an IoT device for environmental monitoring has been reduced using open-source software. A sensor node combining thermal comfort, acoustic comfort, air quality, and visual comfort has been developed in [16], and in [17], the performance of several hardware components for indoor environmental quality has been investigated in a comparative study. Finally, personalized thermal comfort monitoring systems, such as the *climateBOX*, have been developed using low-cost, IoT-based hardware components, emphasizing the important role of sensor calibration to ensure accurate and reliable thermal comfort analysis over time [18].

Assessing thermal comfort only through environmental parameters is challenging due to the large number of physiological and psychological processes affecting the comfort. Therefore, thermal comfort surveys have been used as an alternative to monitoring systems; personal assessments of thermal comfort have been carried out using thermal comfort surveys by obtaining direct feedback from building occupants [19]. Thermal comfort surveys can be conducted manually, but with the rapid advances in digitalization, tools have been made available to incorporate building occupant feedback into thermal comfort assessments in a continuous manner [20]. For example, mobile applications and digital surveys have been implemented to collect feedback on thermal sensations and preferences of building occupants [21]. Smartphone-based applications have been developed, adding visualization tools and real-time interaction between building occupants and the thermal environment [22]. In addition, digital surveys have also been commercialized to assess thermal comfort in the built environment [23].

However, assessing thermal comfort by using either monitoring systems (i.e., environmental data) or thermal comfort surveys (i.e., building occupant feedback) presents certain limitations. On the one hand, only collecting environmental data is not sufficient to assess thermal comfort accurately for every building occupant in an indoor space. On the other hand, assessing thermal comfort only through surveys is time-consuming and involves a regular and reliable participation of building occupants. Therefore, a promising solution to address the aforementioned limitations is to combine both approaches, i.e. environmental data monitoring and building occupant feedback, using new technologies to improve data collection processes. Several studies have incorporated wearable sensors, such as sport watches and smartphones, to obtain personalized thermal comfort data from users and the surrounding environment [24], measuring heart frequencies and activity levels [25]. With the use of wearables, building occupants act as “human sensors” of the built environment, collecting data over long periods of time [26]. To obtain long-term feedback from building occupants, other studies have introduced physical devices as occupant voting systems [27], studying the thermal sensation in relation to some environmental and personal parameters [28]. Moreover, some approaches have addressed the spatial distribution of multiple devices to create thermal comfort monitoring systems [29] and have been compared to other monitoring systems in different indoor environments [30].

Further research has focused on personalized thermal comfort as a way of reducing energy consumption in buildings caused by centralized heating, ventilation, and air conditioning (HVAC) systems, over which building occupants have no control [31]. In the study, the energy consumption and the effect on thermal comfort of four heating devices installed around a desk have been tested. Occupants were free to control (turn on or off) the levels of each heating device. To gain control of the thermal environment, several hardware solutions have been developed to personalize comfort by acting on the thermal environment near individual building occupants while improving energy efficiency in buildings, focusing on rule-based and model-predictive control systems [32]. The study has pointed out the low level of preparation of HVAC systems to be controlled. In [33], an office chair with heating and cooling capabilities has been used as an example of a personalized comfort system (PCS). The paper evaluates the PCS comparing a building controller with adaptive temperature setpoints between 18 and 26 °C to a basic controller with a fixed and narrow setpoint range between 21 and 24 °C. As an alternative of centralized ventilation, the efficacy of different personalized ventilation systems has also been investigated [34,35], in which occupants can manually turn on and off different personalized ventilation systems installed on a desk to reduce air pollutants. As an alternative of a centralized heating and cooling, a heating and cooling wall has been tested under laboratory conditions using a climate chamber and a thermal manikin to study its effect on the different parts of the human body [36]. The heating and cooling wall is divided into three horizontal thermal zones, which can be independently controlled by the user through a mobile app. In the majority of the previously mentioned studies on personalized thermal comfort systems, the control over the environment with HVAC systems or personalized systems has been conducted manually by building occupants. However, autonomous control of HVAC systems is emerging as a research field, using methods and algorithms such as PID controllers, fuzzy logic, particle swarm optimization, and multi-agent systems [37], as well as reinforcement learning [38].Thus, personalized comfort systems are a promising alternative to HVAC systems to reduce energy consumption in buildings without sacrificing occupant thermal comfort. However, further investigation on methods to personalize comfort while reducing energy consumption in buildings is required, as well as monitoring systems dedicated to the further autonomous control of personalized comfort systems using control strategies based on thermal comfort preferences of building occupants.

In summary, a fully digitalized and automated workflow that integrates both environmental data and building occupant feedback is necessary to reduce data loss, time and effort, as well as cost of thermal comfort assessments. Furthermore, by automating data collection, the quality of the data improves and can be integrated in control systems or personalized comfort systems, to maximize comfort while minimizing the energy consumption of buildings. Current approaches, however, have only been tested under controlled conditions and do not consider real-time environmental data nor the direct thermal comfort feedback of building occupants, which limits the effective application in real-world environments. In addition, commercial tools for evaluating thermal comfort and obtaining feedback from building occupants are expensive, methods and tools are not publicly available or open source, and surveys are not integrated with monitoring systems. The high cost and low integration level of feedback and monitoring systems reduces the possibility of obtaining redundant thermal comfort data in more localized areas, i.e. adjacent to the building occupants, increasing the uncertainty of personalized thermal comfort assessments.

To overcome the limitations of assessing personalized thermal comfort solely with monitoring systems or solely with surveys assessing thermal comfort, this paper presents a low-cost comfort monitoring system that couples environmental data collected by mobile intelligent wireless sensor nodes with a digital thermal comfort survey providing feedback from building occupants. Both sources of data are autonomously integrated to form a personalized profile for each building occupant, in which the thermal preferences are stored along with the indoor environmental conditions. The system presented in this study is built using low-cost hardware components that provide state-of-the-art

IoT features (i.e. wireless capabilities and embedded computational power) and uses open-source software to build and adapt applications for thermal comfort assessments as needed for individual use cases. The thermal comfort monitoring system, consisting of

a. intelligent wireless sensor nodes,
b. a portable main station, and
c. a digital thermal comfort survey,

is designed to maximize the collection of environmental data and occupant feedback. The intelligent wireless sensor nodes form the so-called *thermal comfort stations*, which establish a distributed monitoring system based on low-cost hardware components with IoT capabilities. The low-cost hardware components, mainly sensors and microcontrollers, enable the thermal comfort station to compete in price (~50 EUR) with the low-cost sensor nodes with IoT capabilities developed in previously mentioned studies. Each thermal comfort station (CS) is assigned to a building occupant, obtaining redundant thermal comfort data in more localized areas adjacent to the building occupants. In addition, each building occupant has access to the digital thermal comfort survey through a web application, created by a web server hosted in the portable main station. The feedback provided by building occupants through the survey is used to continuously assess personalized thermal comfort over time, and the data is stored in standard formats to ease the import in other software applications for further analyses. By merging and synchronizing environmental data and occupant feedback, and making the information available in standard formats, future surveys will be enabled to statistically analyze the data to study different aspects of thermal comfort, such as the relationship between the determining parameters (environmental and personal) and the subjective measures (such as productivity, thermal preference, and actual thermal sensation), and the interaction of building occupants with the built environment (i.e. with fans, windows, shades, and lights). Ultimately, the thermal comfort monitoring system creates individual profiles for each building occupant by forming a collection of thermal comfort data over time.

The remainder of the paper is structured as follows. First, the development of the low-cost thermal comfort monitoring system is presented, i.e., the system architecture, the hardware and software components of the thermal comfort stations, and the digital thermal comfort survey. Then, calibration experiments performed in a climate chamber are described to demonstrate the accuracy of the low-cost sensors, which are an integral part of the system. The low-cost sensors are calibrated by placing the thermal comfort stations in the climate chamber alongside high-precision sensors that are used for reference, and comparing data collected for different environmental conditions. Next, the capability of the thermal comfort monitoring system to personalize thermal comfort is validated through a field test in an office environment and the results of the validation are presented and discussed, including advantages of the system, and limitations of the study, as well as further recommendations. The paper concludes with a summary of the study, as well as with an outlook on potential future research directions.

## 2. Design and implementation of the thermal comfort monitoring system

This section presents the system architecture of the thermal comfort monitoring system, which describes the components of the system and the relations and communication among the components (Section 2.1). Then, the hardware components (Section 2.2), the software embedded into the intelligent wireless sensor nodes (Section 2.3), and the digital thermal comfort survey (Section 2.4) are elucidated in detail. Finally, the web application that displays real-time thermal comfort data in a dashboard is shown (Section 2.5).

### 2.1. System architecture

The thermal comfort monitoring system presented in this paper is based on a four-layer IoT architecture [39] and takes advantage of abstract modeling of intelligent structural systems [40], embedded computation [41], and smart sensor technologies [42]. The thermal comfort monitoring system includes:

a. thermal comfort stations with its sensors and embedded software applications
b. a portable main station hosting a web server, and
c. the digital thermal comfort survey tool

The thermal comfort stations consist of wireless sensor nodes built with low-cost hardware components. The main reason for using low-cost hardware are possible future applications in large thermal comfort studies, where many stations will be needed. The software applications embedded into the thermal comfort stations integrate algorithms implemented for real-time sensing, embedded data processing, and IoT connectivity. The portable main station consists of a Raspberry Pi (RPi) hosting a web server, which handles the communication of the system, integrates and structures the thermal comfort data, and creates the digital thermal comfort survey and the dashboard where the thermal comfort data is displayed. The digital thermal comfort survey is designed to be completed by building occupants while performing regular office tasks with minimal disruption. The goal of the system is to automate the collection of environmental data and complement the data with the feedback of building occupants enabling personalized thermal comfort assessments in real time.

The architecture of the low-cost thermal comfort monitoring system, shown in Fig. 1, consists of four layers,

(i) an application layer,
(ii) a middleware layer,
(iii) a physical layer, and
(iv) a security layer,

which are depicted in Fig. 1. Building occupants interact with the *application layer* through a dashboard accessible through a web application. The dashboard provides real-time visualization of environmental data and it contains the digital thermal comfort survey. The *middleware layer* contains the portable main station, which hosts a web server based on a RPi, chosen for this study because of the relative low price compared to other portable computers. The main station manages the backend services of the system, i.e. data communication, data management, and data visualization. The backend services are implemented using the Node-RED development tool, a framework that provides visual, flow-based programming for developing the backend logic of systems [43]. Node-RED receives building occupant feedback through the application layer and stores survey results and environmental data collected by the physical layer. The *physical layer* of the automated thermal comfort monitoring system consists of the thermal comfort stations that collect indoor environmental data, i.e. $t_a$, $RH$, $v_a$, and the globe temperature. In addition, the wireless sensor nodes provide computing capacities necessary to process the raw environmental data using embedded algorithms. For example, $MRT$ is computed from the globe temperature, which is used with the other indoor environmental data to compute the PMV and PPD thermal comfort indexes onboard the sensor nodes. The data processed on board is sent to the main station belonging to the middleware layer using an HTTP communication protocol for data storage and visualization. Finally, the *security layer* is devised transversely to the other layers and provides authentication services for privacy and security of all layers as follows. First, the thermal comfort monitoring system is part of a local Wi-Fi network, accessible only with distinct username and password to prevent unauthorized access. Similarly, access to the middleware layer is secured by an

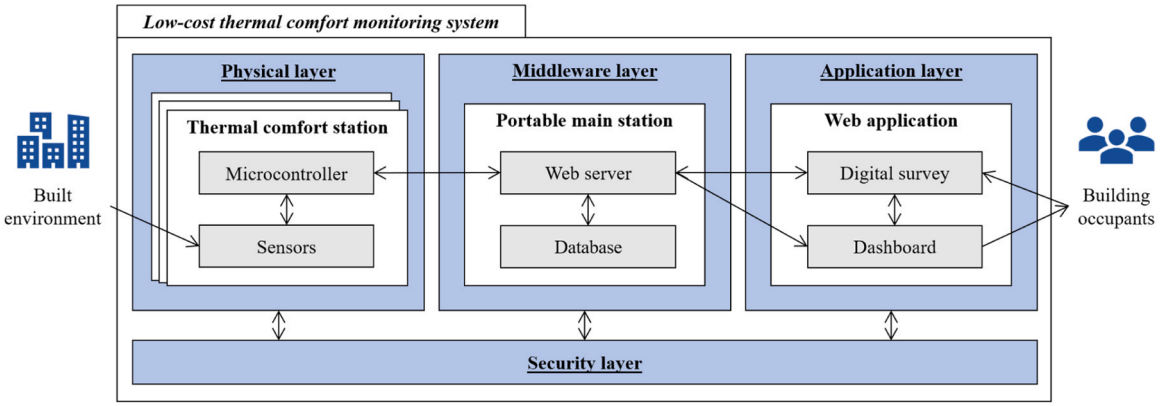


**Fig. 1.** Four-layer IoT architecture of the low-cost thermal comfort monitoring system.

additional password and username, to protect the backend logic and the data. Finally, the web application of the application layer, as part of the local network, is equally protected by the password of the local network, and only individual building occupants with administrative rights are given the URL that grants access to the dashboard and the digital survey.

### 2.2. Hardware components of the thermal comfort station

The thermal comfort stations include three low-cost sensors, (1) a combined sensor that measures $t_a$ and *RH*, type SiliconLabs Si7021 [44], (2) a $v_a$ sensor, type Modern Device Rev. C [45], and (3) a temperature sensor, type B+B Sensors TSic 206-TO92 [46], which is installed in a black-painted table tennis ball, forming a globe thermometer used to measure the globe temperature and to calculate the *MRT*. An ESP32 microcontroller, type Espressif WROOM-32 [47], handles processing of the raw environmental data and periodically sends the data to the middleware layer via Wi-Fi using an HTTP protocol. The sensors and the microcontroller have been selected based on the following criteria: Low price, low power consumption, size, and operability at 5 V. The response times of the low-cost sensors also fulfill the requirements of thermal comfort standards, which require measurements every 3 minutes. For example, the air temperature sensor has a response time of 0.7 s when unmounted and of 5.1 s when mounted on the boards. The relative humidity sensor has a response time of 18 s, while the temperature sensor used to estimate the globe temperature and the air velocity sensor do not share specific numbers regarding response times, although the manufacturer of the air velocity sensor recommends a warm-up period of 10 s for obtaining accurate measurements. is Table 1 summarizes the technical characteristics of the low-cost hardware components used in this study, including the prices. The final price of each thermal comfort station is less than EUR 50, while the price of the Raspberry Pi used for the portable main station is EUR 52, for a total price of 100 € for a system with one thermal comfort station and one portable main station of EUR 100. As shown in Fig. 2a and Fig. 2b, all components are wired to a printed circuit board (PCB), to optimize the stability of the measurements. The figures show the design of the PCB, illustrating the PCB as manufactured. The abovementioned hardware components are placed on the PCB, forming an electrically stable circuit. Stable electrical circuits are important in monitoring systems to avoid sensor faults and to improve the reliability of the measurements taken by the thermal comfort stations. To connect the sensors to the PCB, pitch connectors, type JST PH connector [48], are soldered to the PCB. The sensors are equipped with the appropriate pair connector, type JST EH [49], to mount the sensors to the PCB. The pitch connectors allow jumper wires with crimps to be connected to a strong (yet not soldered) bond between the sensors and the PCB to ensure a good connection under vibrations and mechanical forces, and when used with low voltages and low currents. Moreover, the low-cost sensors are easier to replace by crimping rather than soldering to the PCB.

A 3D-printed enclosure protects the hardware components of the thermal comfort stations. Fig. 3 shows the final aspect of the thermal comfort stations developed in this study, after enclosing the hardware components and the PCB in the 3D-printed case. The design of the case includes bolts in the main body that allow the lid or top of the enclosure

**Table 1**
Hardware components of the thermal comfort stations. Total price for a system with one thermal comfort station and one portable station at the time of purchase for this project.

| Parameter | Manufacturer | Model | Range | Accuracy | Resolution | Power consumption | Dimensions | Price |
|---|---|---|---|---|---|---|---|---|
| $t_a$ | Silicon-Labs | Si7021 | −40 °C to +125 °C | ±1 °C | 0.01 °C | 150 µA | 17.8 mm × 15.3 mm × 3 mm | 10.00 € |
| *RH* | | | 0–100 % | ±3 % | 0.01 % | | | |
| $v_a$ | Modern Device | Rev. C (Hot-wire anemometer) | 0 m/s to 26.67 m/s | - | < 0.0001 m/s | 20 µA to 40 µA | 17.3 mm × 40.4 mm × 6.4 mm | 21.95 € |
| *MRT* | B+B sensors | TSic−206 (Semiconductor-based) | −50 °C to 150 °C | ±0.5 K | 0.1 K | 45 µA | 3.8 mm × 4.6 mm × 2.3 mm | 7.13 € |
| Microcontroller | Espressif | WROOM−32 | - | | - | 50 mA | 25.5 mm × 18 mm × 3 mm | 5.00 € |
| Portable main station | Raspberry Pi | 4B 2 GB | - | | - | 1000 mA | 90 mm × 60 mm × 25 mm | 52.00 € |
| Case | Prusa | PLA | - | - | - | - | 33 m of filament | 3.00 € |
| Other small hardware components | | - | - | - | - | - | - | < 1.00 € |
| Total price | - | - | - | | - | - | - | ~100 € |

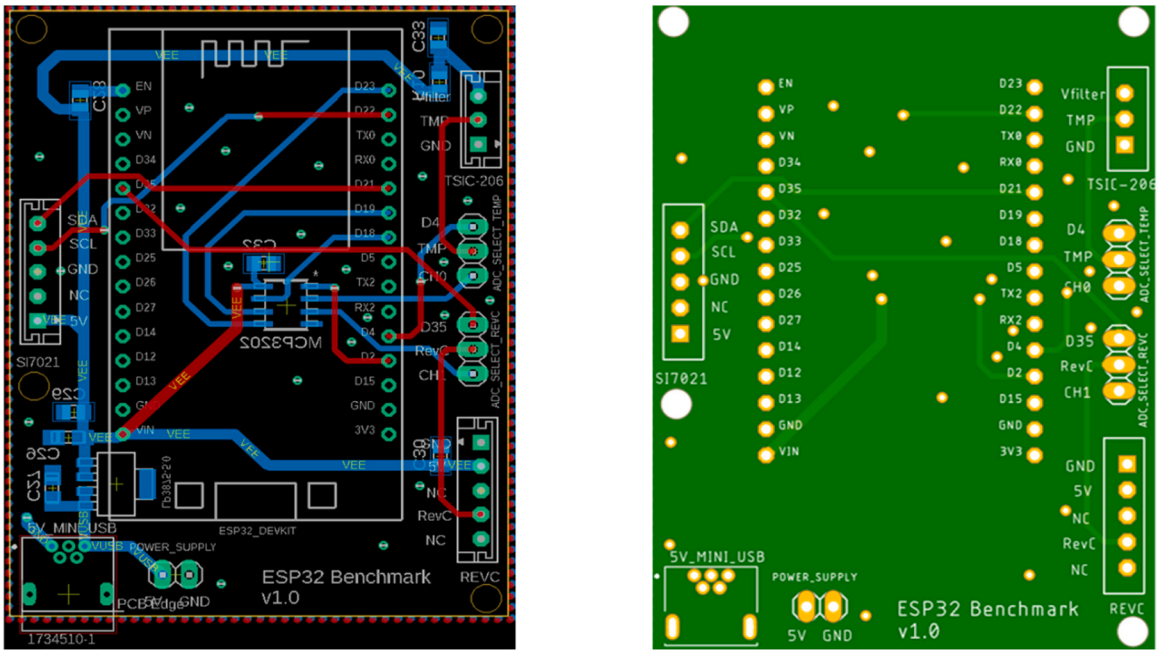


a) Design of the PCB layout. b) Manufactured PCB.

**Fig. 2.** PCB of the thermal comfort station.

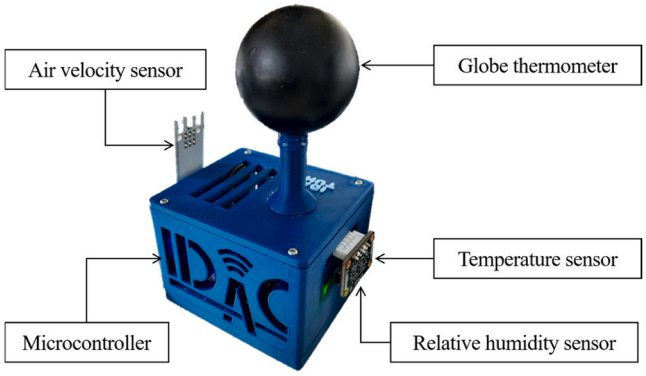


**Fig. 3.** The thermal comfort station.

to be screwed into place. Similarly, the bottom of the main body includes bolts to screw the PCB board to the case and fix all the components of the thermal comfort station. The case comprises several openings to permit the heat generated by the microcontroller to dissipate. In addition, the size of the openings has been designed to mechanically adjust the pitch of the connectors linking the sensors to the PCB and to secure the hardware to the case without the need for glue or any other permanent bonding method. The temperature and humidity sensor is placed as far away as possible from the microcontroller, since it can heat up and affect the measurements. Similarly, the globe thermometer is placed as far as possible to minimize the impact of radiant and convective heat loss of the microcontroller. Additionally, the tube that holds the table tennis ball is filled with glue to prevent convective airflow from entering the globe from the inside. The air velocity sensor is also installed as freely as possible with a distance from the station to avoid the impact of the boundary layer of the station.

### 2.3. Software description

As described earlier, the thermal comfort monitoring system consists of several thermal comfort stations and a portable RPi-based main station. In this subsection, the software embedded into the thermal comfort monitoring stations and the software embedded into the main station will be described.

#### 2.3.1. Software embedded into the thermal comfort stations

The microcontroller of the thermal comfort stations embeds the software application designed to collect sensor data and to exchange environmental and thermal comfort data with the main station. In addition, the software application is designed to calculate the PMV and PPD indexes onboard the microcontroller to predict the average thermal comfort of building occupants in indoor environments. The algorithms for calculating the PMV and PPD indexes are implemented following and adapting the pseudocode available in the ASHRAE Standard 55–2020 [50]. As shown in Fig. 4, the parameters required to calculate the PMV and PPD indexes are (1) the four environmental parameters measured by the thermal comfort stations, i.e. the $t_a$, the $RH$, the $v_a$, and the $MRT$, and (2) the two personal parameters that quantify the insulation level of clothing ensembles ($I_{cl}$) and the metabolic rate, which is associated to the intensity of the activities carried out by building occupants. The personal parameters, entered by the building occupants via the thermal comfort survey, are transmitted to the thermal comfort stations, in which the PMV is calculated as elucidated in Eq. 1a. The PMV is indicated in the 7-point scale from +3 to −3. The PPD index is based on the PMV and is displayed next to it as a function.

The PMV index is updated as soon as new values of either the personal or the environmental parameters, measured continuously by the thermal comfort stations, are available. The output of the PMV index corresponds to a value on a 7-point scale of the ASHRAE Standard 55–2020, where −3 represents cold sensation, +3 represents warm sensation, and an index of 0 expresses neutral thermal sensation. The PPD index is derived from the PMV index, as shown in Eq. 1b.

$$PMV = (0.303e^{-2.1*M} + 0.028) * [(M\text{-}W) - H - E_c - C_{res} - E_{res}] \quad (1a)$$

$$PPD = 100 - 95e^{-(0.03353*PMV^4 + 0.2179*PMV^2)} \quad (1b)$$

In Eq. 1a, the terms, described below, denote the different energy

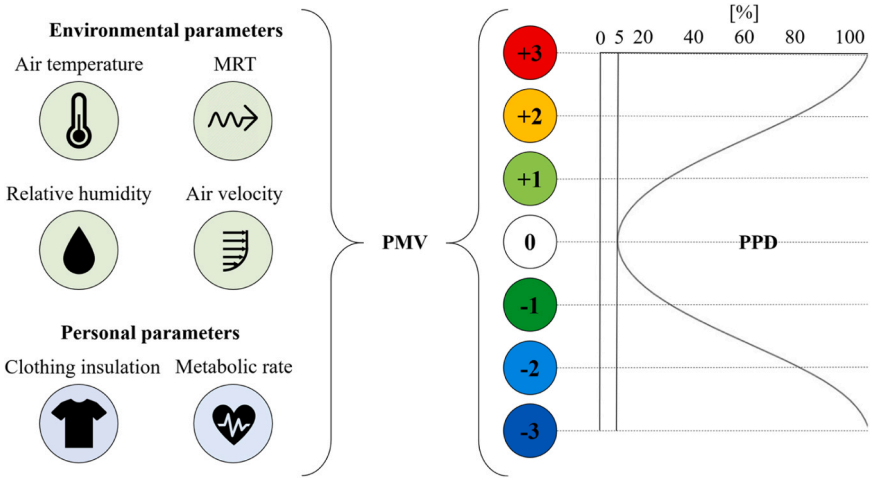


**Fig. 4.** Parameters required for the calculation of the PMV and PPD indexes.

and heat exchanges between the body and the surrounding environment. Pseudocode is available in the ISO 7730 standard [51] to calculate the heat exchange parameters, and ultimately the PMV and PPD indexes. The heat exchanges are derived from the measurements of the environmental parameters and the personal parameters, which are denoted as follows:

$M$ – the metabolic rate, in Watt per square meter (W/m$^2$);

$W$ – the effective mechanical power, in Watt per square meter (W/m$^2$);

$H$ – the sensitive heat losses (W/m$^2$);

$E_c$ – the heat exchange by evaporation on the skin (W/m$^2$);

$C_{res}$ – the heat exchange by convection in breathing (W/m$^2$);

$E_{res}$ – the evaporative heat exchange by breathing (W/m$^2$).

The software applications embedded into the thermal comfort stations are implemented in C++ and with high-level Arduino functions, which are compatible with the microcontroller of the thermal comfort stations. The microcontroller comes with a flash memory of 8 MB, in which most of the flash memory space is reserved for storing the bootloader and the embedded software application code. The code is automatically executed when the thermal comfort stations are powered on and is divided into two main functions, the *setup* function and the *loop* function. The setup function is dedicated to establishing the wireless connection to a Wi-Fi network and to a web server, as well as to initializing the hardware components. The loop function is dedicated to collecting data, aggregating data, analyzing data (i.e. calculating the PMV and PPD indexes), and finally transmitting data and information to the server. The loop function is executed over and over again as long as the thermal comfort stations are supplied with power or the microcontrollers are manually reset. The microcontrollers only hold 512 bytes of flash memory for storing thermal comfort data, thus, the collected data must be transmitted after a certain period of time. According to thermal comfort standards [50,51], environmental parameters must be measured at least every 3 minutes for accurate thermal comfort assessments. To improve the accuracy of the assessments, the thermal comfort stations measure the environmental parameters every 5 seconds and send an averaged value every 3 minutes to lower the variability of the measurements. Unlike other applications (e.g. known from vibration-based monitoring), thermal comfort data collection does not require a high-frequency sampling rate and, therefore, does not require additional memory.

### 2.3.2. *Web server hosted on the portable main station*

Web servers are computer systems that can, e.g., deliver web content to users, host databases, or run web applications. Typically, web servers are hosted in large data centers or server rooms, which include expensive hardware and software services. In this study, however, the web server is hosted by the portable main station of the thermal comfort monitoring system, consisting of the RPi. To enable wireless communication between the thermal comfort stations and the web server, the software application embedded in the microcontroller of the thermal comfort station includes the network location of the RPi that hosts the web server (with IP address and the TCP port).

An HTTP endpoint is implemented using the Node-RED framework to build the web server, as shown in Fig. 5. Node-RED is open source and compatible with the Raspbian operating system of the RPi. By using the Node-RED framework, programmers may implement web servers with a visual programming interface, creating *flows* consisting of predefined *nodes*. In Node-RED, flows are used to implement backend services, i.e. data communication, data management, and data visualization. Flows consist of interconnected nodes, which serve as basic building blocks performing computational actions on the data. Nodes in Node-RED are triggered by either receiving messages from the previous node in a flow, or by waiting for some external event, such as an incoming HTTP request. Nodes process the messages, or events, and then send a message to the next nodes in the flow. A node can have one input and as many outputs as the logic of the flow requires.

In the HTTP endpoint, the RPi-based web server receives the thermal comfort data, i.e. the environmental data, the PMV index and the PPD index, from the $N$ thermal comfort stations $CS_n$ ($n = 1 \ldots N$). As shown in Fig. 5, the node *Get data from CS* listens to HTTP requests, which enable the data communication between each $CS_n$ and the web server. When the request is accepted, a message containing the thermal comfort data is received and forwarded to the *Switch* node. The switch node identifies which thermal comfort station is sending the data by recognizing a unique number that each $CS_n$ carries, which corresponds to the first parameter in the message. In addition, the occupant feedback entered via the digital survey is integrated into the data coming from $CS_n$. The *Switch* node formats the message in a comma-separated-value (CSV) string. The CSV string contains all thermal comfort parameters measured by $CS_n$ and the occupant feedback in a specific point in time, determined by a timestamp. Thereafter, the CSV string is forwarded to the next node, which creates a CSV file for the data received from $CS_n$, forming a document-oriented database. If the file already exists, the CSV string, containing all the thermal comfort parameters, is added to a new line of the CSV file, thus creating a thermal comfort time history, associated with $CS_n$, and a personalized thermal comfort profile for each building occupant. The last node in the flow, the *Send data to* $CS_n$ node, transmits the feedback of building occupants from the web server back to the $CS_n$, which is used for computing new PMV and PPD indexes. Finally, the *Plot in dashboard* node forwards the thermal comfort data to the web application. In particular, building occupants can visualize in real time the thermal comfort data in a dashboard by navigating to a

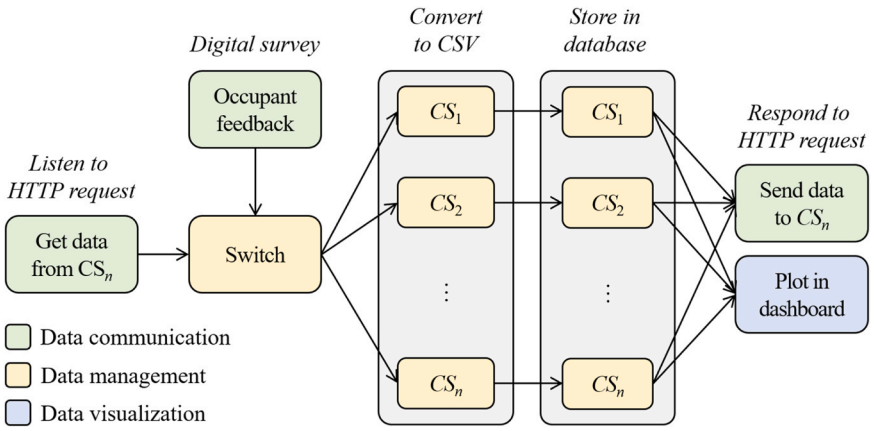


**Fig. 5.** HTTP endpoint implemented on the RPi-based web server using Node-RED.

personalized URL on a web browser. The feedback introduced by the building occupants through the digital thermal comfort survey is described in the next subsection.

### 2.4. Digital thermal comfort survey

The digital thermal comfort survey is devised to collect feedback from building occupants about the thermal environment. To collect the feedback, the building occupants are asked to use the web application on the personal computers or mobile devices connected to the local network. The survey, shown in Fig. 6 for the building occupant associated with station 2, comprises ten fields categorized into

(1) personal parameters,
(2) subjective measures, and
(3) interactions with the built environment.

The parameters align with international thermal comfort standards [50,51] and dedicated literature [52]. The parameters captured by the digital thermal comfort survey are described in detail in the following subsections.

#### 2.4.1. Personal parameters

Before entering the personal parameters, the 1. *Counter* starts the survey and keeps track of the number of times building occupants complete the digital thermal comfort survey. As shown in Fig. 6, occupants need to click on the button to increment the counter. In future, the counter will work automatically. Afterwards, the personal parameters can be entered as follows:

2. *Clothing insulation* ($I_{cl}$) quantifies the clothing ensemble worn by an occupant and its resistance to sensible heat transfer, expressed in units of *clo*. A dropdown menu offers a pre-defined selection of common clothing ensembles worn in offices. Values necessary for PMV index calculations are taken from tables in the ASHRAE Standard 55–2020.
3. *Metabolic rate (met)* quantifies the intensity of different types of office activity performed by a building occupant at the moment of the survey via a dropdown menu. Values for various activities are also derived from the ASHRAE Standard 55–2020. Each office activity type is expressed by a metabolic rate (met) value expressed in *met* units.

The two personal variables (as well as the environmental parameters) are used to calculate the PMV and PPD indexes using "real" values rather than estimations or mean values, which is one of the strengths of the thermal comfort monitoring system. Other personal parameters such as gender, age, weight, and origin may also have an influence on the thermal comfort perceived by building occupants; As they are not required to calculate the PMV index and to comply with data privacy

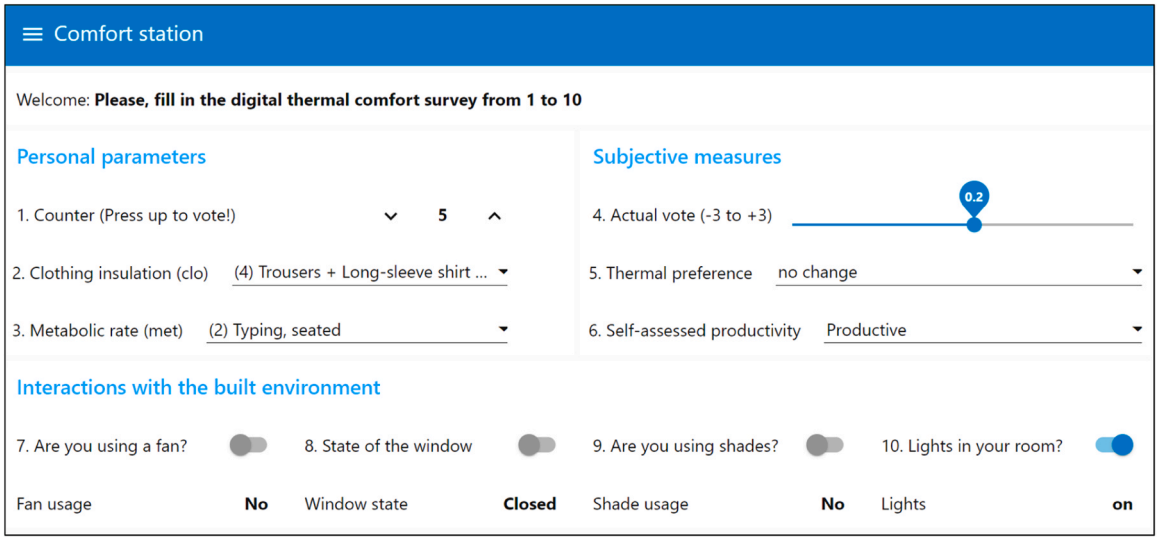


**Fig. 6.** Prototype of the digital thermal comfort survey, as part of the web application.

regulations, they are not considered in the digital survey. Nevertheless, additional parameters may be added to the web application using the Node-RED framework, if required.

#### 2.4.2. Subjective measures

Three subjective measures are captured via the digital thermal comfort survey, which are detailed as follows:

4. *Actual vote (thermal sensation vote)* describes how the building occupants feel on the ASHRAE 7-point thermal comfort scale, which mirrors the PMV index representation. The actual vote, often considered ground truth feedback, offers direct occupant input on their thermal comfort. The web application hosting the digital survey displays a slider spanning −3 to +3, enabling occupants to select values in 0.1-point increments.
5. *Thermal preference* represents the preference of building occupants for the environment through three qualitative options in a dropdown menu: “I would prefer to be warmer”, “I would prefer to be cooler”, or “no change”. The thermal preference aims to discover which thermal conditions are preferred by a building occupant, considering that under the same thermal environment, occupants might have different thermal preferences.
6. *Self-assessed productivity* measures the self-rated productivity on a 5-point scale. Options, selected from a dropdown menu in the digital survey, include: “Unproductive”, “not very productive”, “normal”, “productive”, and “very productive”. The parameter of self-assessed productivity aims to evaluate the impact of thermal comfort on occupant productivity.

#### 2.4.3. Interactions with the built environment

In this category, the interactions of building occupants with the built environment are captured through four parameters. The four parameters captured for this study are related to the following elements commonly used in the built environment to thermally adapt to the surroundings. However, any other parameters can be added to the system to conduct concrete studies related to the built environment, for example, adding the use of PCS, such as heating or cooling walls or office chairs.

7. *Fans*: Occupants can indicate fan usage via a simple switch button in the user interface, collecting a “yes” or “no” response.
8. *Windows*: Building occupants can select the window state (open or closed) by toggling a switch button in the system.
9. *Shades*: The user interface displays a switch from which the building occupant can select if shades are up or down.
10. *Lights*: A switch button can be used to measure the use of artificial lighting.

### 2.5. Visualization of the thermal comfort parameters

Fig. 7 shows the dashboard that, on the one hand, provides building occupants with a visualization of the four environmental parameters, i.e. the $t_a$, the *RH*, the $v_a$ and the *MRT*, continuously measured by the thermal comfort stations. On the other hand, the dashboard displays the thermal comfort indexes relevant to this study, i.e. the PMV index, the PPD index, and the actual vote, which represents the actual thermal sensation experienced by a building occupant. The data collected by the digital survey is merged with the environmental data, continuously collected by the thermal comfort stations. Then, the environmental data and the feedback obtained through the survey are automatically stored in CSV files in the portable main station by the web server of the thermal comfort monitoring system.

## 3. Calibration of the thermal comfort stations

Calibrating the low-cost sensors prior to the deployment in real-world environments is essential to ensure the quality of the measurements. This section describes the experiments for calibrating the sensors of the thermal comfort monitoring stations. First, the setup of the experiment, carried out in a climate chamber and using high-precision sensors for reference, is described. Then, the results of the calibration experiment and the accuracy of the low-cost sensors in relation to the high-precision sensors are explained and discussed.

### 3.1. Experimental setup

The low-cost sensors of the thermal comfort stations are calibrated in a climate chamber with a size of 3 m × 3 m × 2.44 m located in a 5.4 m × 5.4 m × 3.05 m laboratory hall to keep it isolated from the outdoor conditions (Fig. 8). The chamber is built using insulated sandwich panels with an overall heat transfer coefficient of $U = 0.27$ W/m$^2$K, which provides a high level of thermal insulation from the surrounding room. The chamber is tempered by water-bearing capillary tubing placed under the interior finishing surface, which consists of tiles for the floor and gypsum plaster for walls and ceiling. The door is not tempered, yet due to the low overall heat transfer coefficient ($U = 0.29$ W/m$^2$K) and the rather small $t_a$ difference between the two sides of the door, it is assumed that the non-tempered door does not strongly impact the air or surface temperatures in the chamber. The temperature in the chamber can be set between 10 °C and 40 °C by controlling the temperature of each surface separately and/or by setting the temperature of a ventilation system installed in the chamber. The chamber then adjusts the inlet temperature or the temperature of the surfaces (or both), to achieve the user-specified $t_a$. Centered inside the climate chamber, the reference sensors and a wind tunnel are placed along the thermal comfort stations for carrying out the calibration experiments. The user interfaces to control the process of the experiments are located outside the chamber. The setup of the low-cost system and the reference system installed in the climate chamber is illustrated in Fig. 8.

To calibrate the low-cost thermal comfort monitoring stations, conventional, proprietary high-precision sensors are deployed, serving as reference sensors. The specifications of the conventional proprietary sensors, the subsections describing the calibration experiments, and the low-cost sensor calibrated against each reference sensor are listed in Table 2. The reference sensors, supplied by Ahlborn, Germany, are

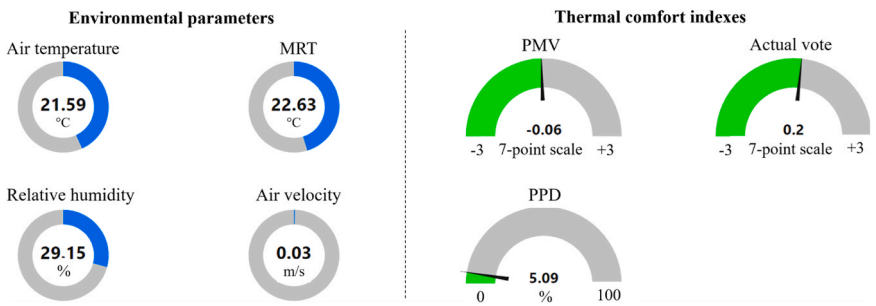


**Fig. 7.** Dashboard of the thermal comfort monitoring system, including real-time charts of the environmental parameters and the thermal comfort indexes.

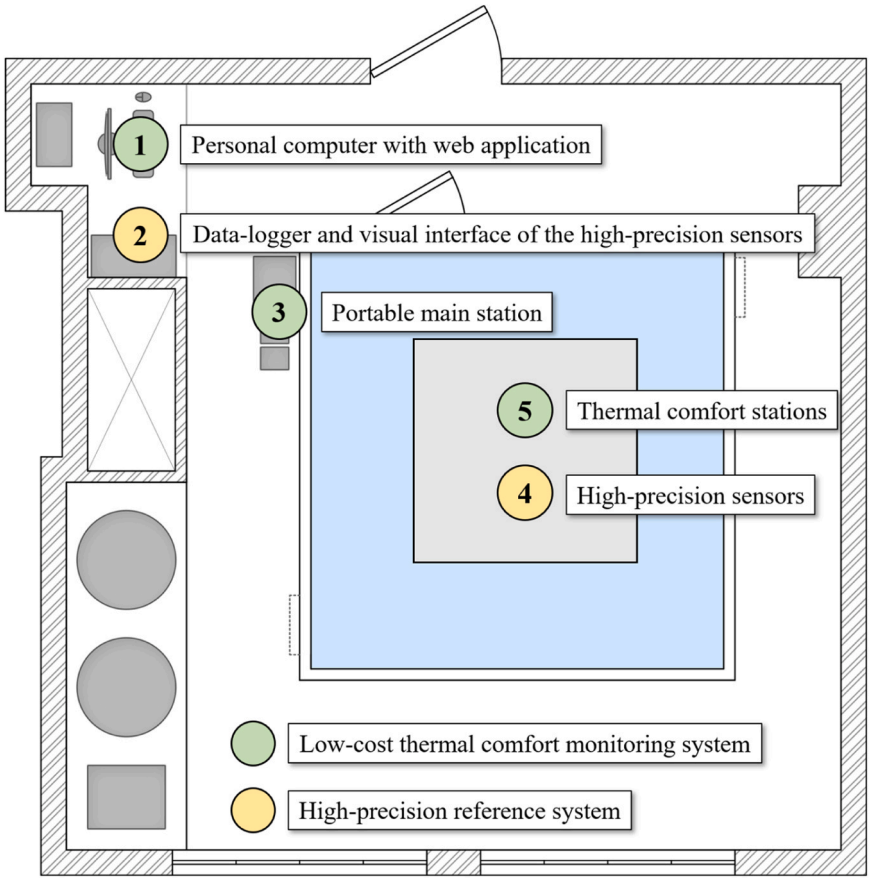


**Fig. 8.** Experimental setup of the calibration experiments conducted in the climate chamber.

**Table 2**
Reference sensors used in the calibration experiments in the climate chambers.

| Section | Parameter | Reference sensor model | Accuracy | Resolution | Range | Low-cost sensor |
|---|---|---|---|---|---|---|
| 3.2.1 | $t_a$ | NTC Type N | ±0.2 K | 0.01 K | −20 °C to 100° C | Si7021 |
| 3.2.1 | *MRT* | 150 mm black globe with Pt100 element | ±(0.3+0.005\|T\|) K | 0.01 K | −40 °C to 200 °C | TSic 206-TO92 |
| 3.2.2 | *RH* | Capacitive sensor | ±2 % *RH* in the range of 10–90 % RH | 0.1 % | 5–98 % | Si7021 |
| 3.2.3 | $v_a$ | Omnidirectional thermo-anemometer | ±(1 % of final value + 1.5 % of measured value) | 0.001 m/s | 0.01 m/s to 1 m/s | Rev. C |
| | | Omnidirectional thermo-anemometer | ±(1 % of final value + 3 % of measured value + 2 digits) | 0.001 m/s | 0.05 m/s to 2.5 m/s | |

connected to a central data logger, type Almemo MA5990–0 positioned at the control station outside the climate chamber. In addition to the data logger, the reference system incorporates the AMR WinControl software [53], consisting of a user interface for graphical representation of the measurements and export of thermal comfort data in different formats. The reference sensors include (i) an $t_a$ sensor (Almemo FN0001K [54]), (ii) a humidity sensor (Almemo FHA646-E1 [55]), (iii) a globe thermometer (Almemo FPA805GTS [56]), and (iv) two $v_a$ sensors (Almemo FVA605-TA1O [57] and Almemo FVAD05TOK300 [58]. To compare the reference sensors to the monitoring stations, all sensors are placed next to each other on a table at the center of the climate chamber, as shown in Fig. 9. The height of the centerline of the sensors is located at 1.2 m above the floor and 1.5 m from the side walls. Particularly for the air velocity calibration, a 2 m long wind tunnel, consisting of a motor and a tube, is placed at a height of 0.75 m. To obtain meaningful results of the calibration experiments, the measurements are conducted under different boundary conditions, including the common environmental conditions present in regular offices, as described in Subsection 3.2 for the calibration experiments of each low-cost sensor.

### 3.2. Results of the calibration of the low-cost sensors

The results of the calibration of each low-cost sensor included in the thermal comfort stations are described and, for each sensor type, depicted in the following subsections.

#### 3.2.1. Calibration of the temperature sensors

To calibrate the sensors, the four walls, the floor, and the ceiling of the climate chamber are set to a specific temperature. The climate chamber is considered to have achieved a stationary temperature when the reference temperature sensor, placed in the center of the chamber, has reached the temperature set on all surfaces. Reaching steady state is monitored from the exterior of the climate chamber and helps reducing to the non-uniformities inside the climate chamber to ensure optimal conditions for calibrating the low-cost sensors.

In Fig. 10, the results of calibrating both low-cost sensors measuring air and globe temperature using four thermal comfort stations are depicted, with the different phases of the experiment numbered. For calibration, the climate chamber is set to a stationary temperature of 18

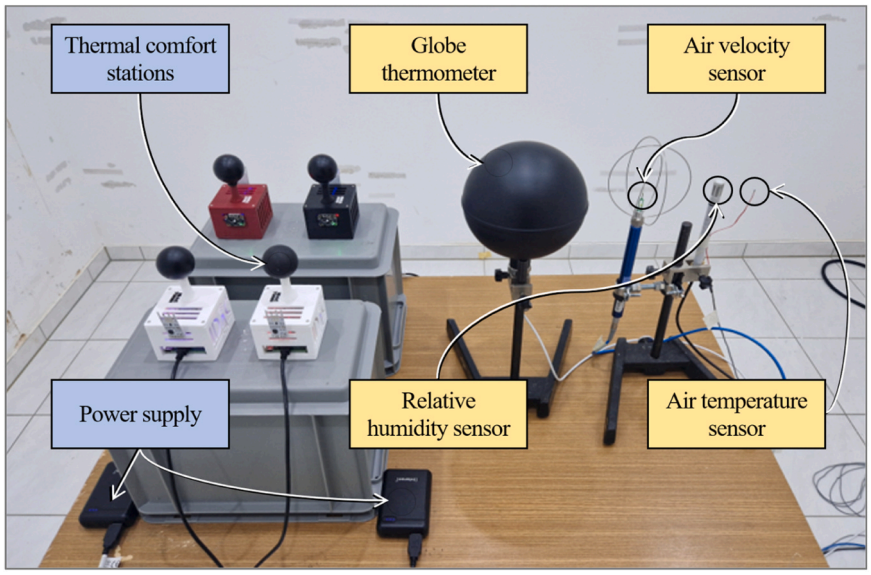


**Fig. 9.** Experimental setup and the location of the thermal comfort stations (blue) and the high-precision sensors used for reference (yellow) in the climate chamber.

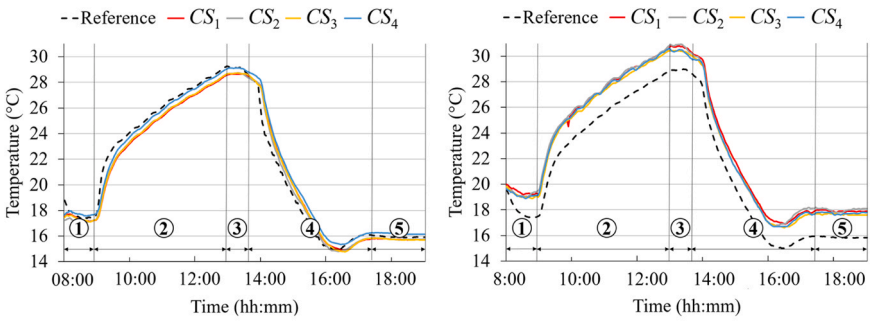


**Fig. 10.** Calibration results of the temperature sensors, including the phases of the experiment.

°C (phase 1). Then, the climate chamber is set to 28 °C. The air and globe temperature are measured in a transient phase (phase 2), due to the time it takes for the climate chamber to reach 28 °C. Phase 2 is followed by phase 3 after reaching 28 °C. As the climate chamber takes a long time to reach steady state, this phase is short. For the calibration, the short time of phase 3 is unimportant as all sensors are exposed to the same environment since the beginning of the experiment. Thereupon, the chamber is set to 16 °C, initiating another transient phase (phase 4), this time representing a descending temperature phase. Finally, the low-cost sensors and the reference sensors measure the air and globe temperature at a stationary climate chamber temperature of 16 °C (phase 5). The sampling frequency used to measure the temperature parameters with the low-cost and the reference sensors is of 1 Hz.

From the data collected during the experiment, it can be concluded that the offset of the values of the low-cost $t_a$ sensors is smaller than the offset observed in the globe thermometers when both groups of sensors are compared with the corresponding reference sensor. The average offset of $t_a$ and $t_g$ is obtained by subtracting the mean value of $t_a$ and $t_g$ measured by the four thermal comfort stations from the value measured by the reference sensor. The average offset of the $t_a$ sensors during the calibration experiments corresponds to $\bar{t}_a = 0.221$ °C, and the average offset of the globe temperature is $\bar{t}_g = -1.86$ °C. The offsets of both the low-cost air temperature sensor and the globe thermometer affect the value of the PMV slightly. For example, as shown in Table 3, with the parameters measured in Case 1, the PMV = −0.10. With an uncalibrated air temperature sensor (Case 2), the PMV index under the same conditions, would have shown a value of −0.06, which corresponds to a 0.04 difference in the PMV index. In Case 3, having a hypothetical uncalibrated globe thermometer and assuming $v_a = 0$ (where the $t_g$ = MRT), a PMV index of +0.19 would have been measured, corresponding to an absolute difference of 0.29. Due to the inaccuracies in the assessment of thermal comfort when using uncalibrated environmental sensors to compute models such as the PMV, both the air temperature sensor and the globe thermometer are calibrated by adjusting the offset in the software program embedded in the microcontrollers of the thermal comfort stations.

**Table 3**
Exemplary effect of inaccurate measurement of the PMV index due to uncalibrated sensors.

| Case | $t_a$ | MRT | RH | $v_a$ | Clo | Met | PMV | Difference |
|---|---|---|---|---|---|---|---|---|
| 1 | **25** | **25** | 50 | 0.00 | 0.61 | 1 | **−0.10** | 0 |
| 2 | **25.221** | 25 | 50 | 0.00 | 0.61 | 1 | **−0.06** | 0.04 |
| 3 | 25 | **26.86** | 50 | 0.00 | 0.61 | 1 | **+0.19** | 0.29 |

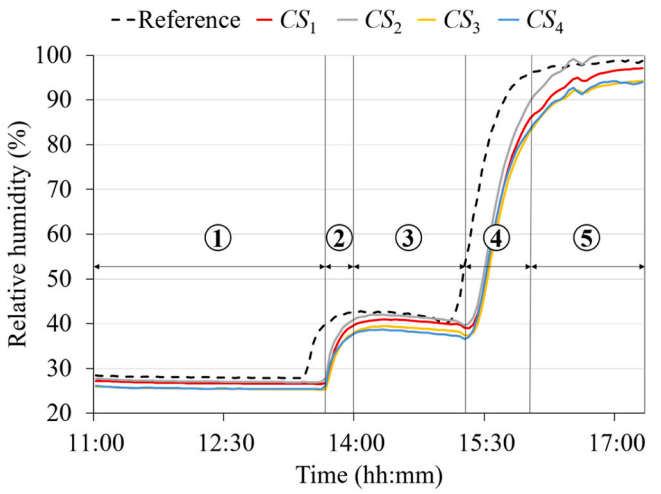


**Fig. 11.** Calibration curves of the humidity sensors, including the phases of the experiment.

### 3.2.2. Calibration of the relative humidity sensor

The control system of the climate chamber cannot regulate *RH*. Thus, the calibration of the low-cost humidity sensor is conducted using a humidifier device that elevates the indoor *RH*. The *RH* is measured in the chamber first without influence of the humidifier (to obtain a reference value) and then under increasing humidity conditions until reaching saturation, i.e. $RH = 100$ %. Fig. 11 shows the experiment for calibrating the low-cost humidity sensor of the thermal comfort stations. As observed in the figure, the experiment consists of three stationary phases and two transient phases between the phases. In the first stationary phase (phase 1), the reference humidity sensor indicates a value of $RH =$ 29 %, while the four low-cost sensors indicate a value of $RH = 27$ %. Next, the humidifier increases the *RH* of the climate chamber until the reference humidity sensor indicates a value of approximately $RH = 40$ % (phase 2), after which the humidifier is stopped, leading to another stationary phase (phase 3). The *RH* is measured for approximately one hour to obtain enough values to compare the accuracy of the low-cost sensors of the thermal comfort stations with the reference sensor. As observed during the transient phases (phases 2 and 4), the reaction time of the low-cost relative humidity sensors is slower than the reaction time of the reference sensor. The slower reaction time of the low-cost sensor happens due to the averaging of relative humidity values collected over 3 minutes with a sampling frequency of 0.2 Hz and computed in the microcontroller of the thermal comfort stations, which does not influence the results of the calibration due to the long and stable measurement periods in the climate change. At higher *RH* values (phase 5 with $\sim RH = 90$ %), the low-cost humidity sensors decrease in accuracy when compared to the reference humidity sensor. As with the air temperature sensor and the globe thermometer, the low-cost *RH* sensor is calibrated by adjusting the offset in the software embedded in the CS, even though small deviations in *RH* only have a minor influence on the calculated PMV and PPD.

### 3.2.3. Calibration of the air velocity sensor

To collect the most accurate indoor measurements possible, one low-cost air velocity sensor is calibrated in a wind tunnel, using high-precision thermo-anemometers as a reference. The low-cost sensor is calibrated for air velocities between $v_a = 0 \ldots 2$ m/s, in steps of 0.1 m/s, collecting a total of 21 calibration points. Two reference sensors were used for the experiment, where sensor (1) was used to calibrate the low-cost sensor from 0 m/s to 1 m/s and sensor (2) from 1 m/s to 2 m/s, as shown in Fig. 12.The wind tunnel, consisting of a radial blower, a tube ($d = 40$ mm), and a fin-type flow straightener, was used to generate laminar air flow with different velocities. The low-cost air velocity sensor is placed at the end of the tube, while two high-precision $v_a$ sensors are embedded inside with the sensing element aligned to the center of the tube, as illustrated in Fig. 12. The two reference sensors are inserted in the wind tunnel with a distance of $l = 0.5$ m, which avoids disturbing the laminar flow inside the tube for this setup.

The geometry of the low-cost sensor is not symmetrical in which the sensing element is located on the flat surface of the sensor board. Therefore, the angle of attack, i.e. the angle at which air flow hits the sensing element, affects the measurement of the $v_a$. Therefore, $v_a$ is measured from four different positions during the experiment: Front, rear, both sides, and top, as shown in Fig. 13. In addition to studying different angles of attack, different temperatures are considered during the calibration experiment. The calibration of the low-cost air velocity sensor is conducted at different temperatures because the sensor is based on a thermistor, whose measurements are temperature-dependent. The *Rev. C* air velocity sensor has been previously calibrated in laboratory experiments in [14], using a test wind tunnel and obtaining a polynomial calibration equation of degree 3, based on the analog values obtained via an ESP32 microcontroller (*RV_ADunits*), the same microcontroller used in this work. *RV_Adunits* are the values of the analog signal received by the pin of the ESP32 microcontroller, which has a resolution of 13 bits for a voltage between 0 and 3.3 V; the analog signal can therefore have values between 0 (for a signal of 0 V) and 4096 (for 3.3 V). The value of the analog signal is proportional to the air velocity. The polynomial calibration equation in [14], which is shown in Eq. 2, was used in the program embedded in the thermal comfort stations. The authors considered the air temperature ($t_a$) and the temperature measured by the thermistor of the *Rev. C* sensor ($t_{RevC}$) for calibration, which is set to a value of $t_{RevC} = 21.9$. In addition, the polynomial equation contains constants with the following values: $K_1 = 15.36921$, $K_2 = 0.01788$, $K_3 = -29.04560$, $K_4 = 1.01536$. Nevertheless, the effect of the air temperature has been tested again in this work under controlled conditions with the help of the climate chamber to ensure maximum accuracy.

$$v_a = \frac{2.285 * RV\_ADunits^3 - 12.417 * RV\_ADunits^2 + 22.831 * RV\_ADunits - 14.19}{K_4 - ((t_{RevC} - t_a) * K_1 * RV\_ADunits^{K_3})) - (t_{RevC} - t_a) * K_2} \quad (2)$$

The diagrams shown in Fig. 14 depict the average air velocities of the angles of the low-cost sensor used during the experiment (blue) and the measurements of the high-precision sensors that are used for reference (green) at different temperatures in the climate chamber. The air velocities are tested in six experiments with at 15 °C, 20 °C, 23 °C, 25 °C, 30 °C and 35 °C, to be able to interpolate with more precision. For each experiment at each of the air temperatures, the air velocity is first adjusted for air velocities of $v_a = 0$ m/s, as it is suggested by the manufacturer of the sensor [45]. The offset at 0 m/s for each of the six experiments is as follows: $offset_{15} = 0.37$, $offset_{20} = 0.27$, $offset_{23} = 0.23$, $offset_{25} = 0.23$, $offset_{30} = 0.18$, $offset_{35} = 0.03$. Then, air velocities between $v_a = 0 \ldots 2$ m/s, in steps of 0.1 m/s are measured. The results confirm that the low-cost sensor measures different air velocities under the influence of different temperatures, as can be seen in the diagrams of

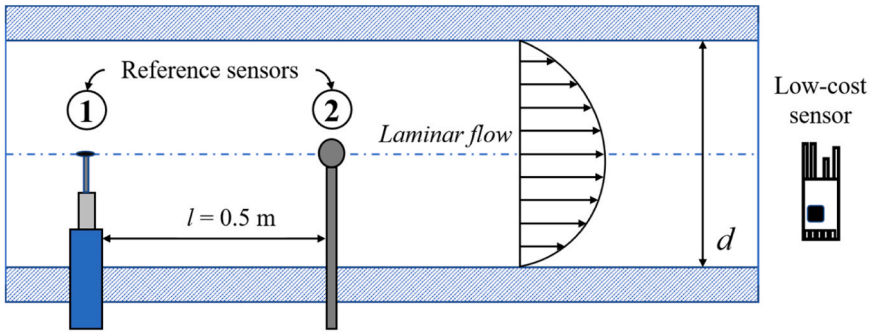


**Fig. 12.** Experimental setup to calibrate the low-cost air velocity sensor. (1) Reference thermo-anemometer ($v_a$ = 0.01–1 m/s), (2) reference thermo-anemometer ($v_a$ = 1–2 m/s).

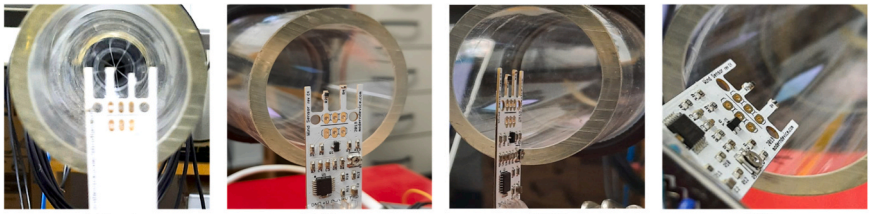


**Fig. 13.** Photos of the calibration experiment for all sides of the air velocity sensor.

Fig. 14, in which the offset between the low-cost sensors and the reference values increase the higher the air velocities are in the six experiments at different air temperatures. For example, the diagram showing the results of the measurements at $t_a$ = 15 °C indicates that, on the one hand, the low-cost sensors measure, in average, a $v_a$ value almost twice as large as the reference air velocity sensor. On the other hand, at

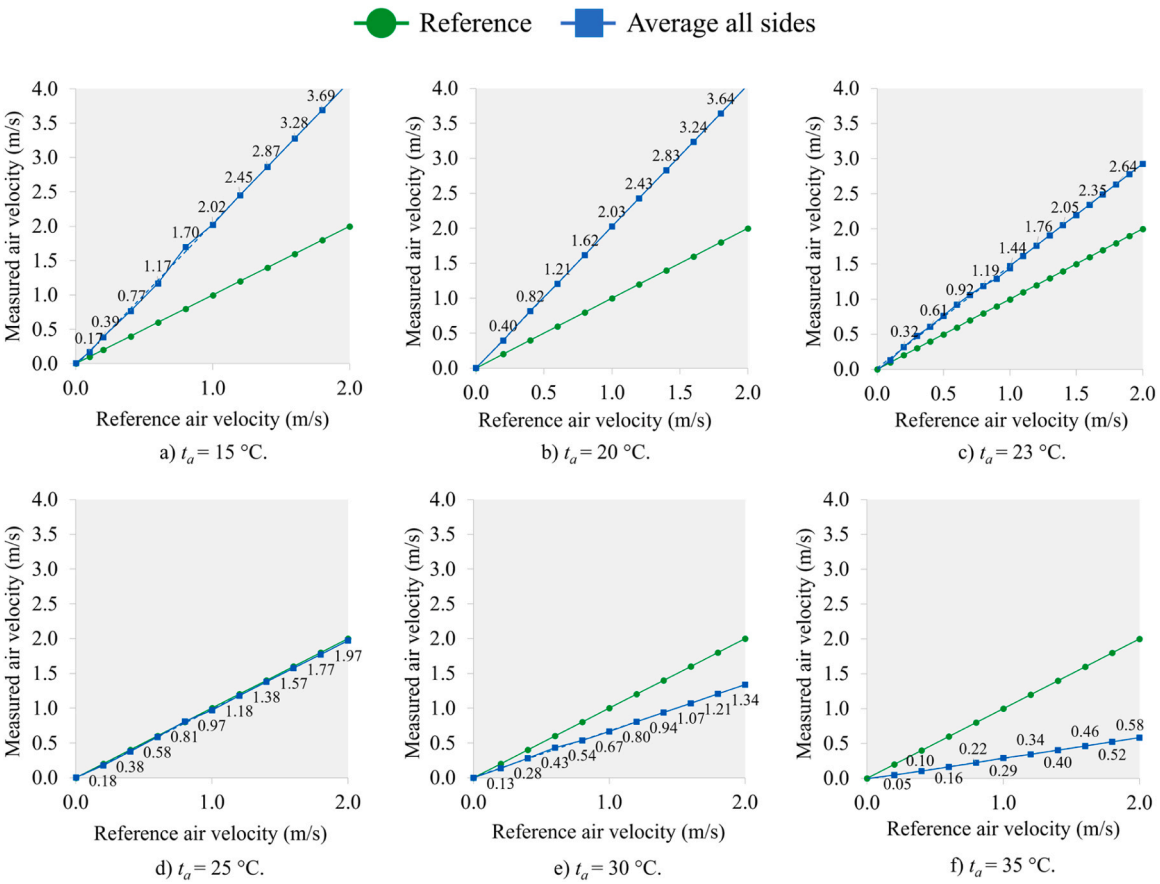


**Fig. 14.** Calibration results for the air velocity sensors at different air temperatures.

$t_a = 35$ °C, the low-cost sensors measure air velocities that are approximately half the value of the reference sensor. At moderate air temperatures ($t_a = 23$ °C; 25°C), however, the low-cost sensor is quite accurate, which indicate that the calibration curves obtained in [14] work well for moderate indoor room temperatures. Moreover, the results shown in Fig. 14 indicate that the inaccuracy of the low-cost sensor readings increases linearly as the air velocities increase. Thus, the calibration curves of the low-cost sensors are adjusted to match the reference values for more sensor accuracy.

After the wind tunnel calibration of one $v_a$ sensor, all low-cost $v_a$ sensors are calibrated and tested in the climate chamber. This is necessary to simulate real world conditions where air flows are omnidirectional and might be subjected to *blocking effects*. In the investigated case, air velocities are quite low as the mechanical ventilation was switched off and only natural convection existed. For testing, the low-cost sensors are compared to the high-precision sensor used for calibration from $v_a = 0$ m/s to $v_a = 1$ m/s. The results of the test of the low-cost $v_a$ sensors are shown in Fig. 15. The four low-cost sensors capture the changes in air velocity that the high-precision sensor measures, as can be seen from the simultaneous peaks in the figure. However, two of the low-cost sensors, $CS_1$ and $CS_3$ measure air velocities with an average offset value of $v_a = +0.25$ m/s, which may be subjected to blocking effects. The air velocity tests highlight that there may be inaccuracies in the calculation of the PMV index due to the uncertainty and the errors induced by the air velocity sensor, which is may be only suitable to a limited extent. The accuracy of the air velocity measurement also influences the MRT value, which is also used to calculate the PMV index, although the error remains small due to the relatively low air velocities in indoor environments. The offset for the air velocity sensor of thermal comfort stations $CS_1$ and $CS_3$ is calibrated before the field test that is described in the next section.

## 4. Validation of the thermal comfort monitoring system

To validate the capability of the low-cost system to monitor occupant thermal comfort, a four-week field test is conducted during the month of April in Germany, which has a moderate continental climate in the spring season, with average temperatures of 9 °C. The field test is conducted in an office environment during regular office activities under real-world conditions. The thermal comfort monitoring system collects (i) environmental parameters measured by the thermal comfort stations and (ii) feedback from the building occupants entered through the digital survey, comprising (1) personal parameters, (2) subjective measures, and (3) interactions with the built environment. In the following subsections, the test setup is introduced, followed by the presentation and a discussion of the results.

### 4.1. Field test setup

The field measurements were conducted at five office rooms located in an office environment. The measurements were performed using the four previously-mentioned thermal comfort stations in addition to a fifth station, which was constructed and calibrated after the calibration of the four other stations. The thermal comfort stations measure the four environmental parameters, i.e. $t_a$, $RH$, $v_a$, and $t_g$ (to calculate $MRT$) at 5-second intervals during three minutes before sending an average for each parameter. The averaged environmental parameters are used to calculate the PMV index, which is calculated onboard the thermal comfort station and sent to the server every three minutes. Each station collects data for 4 weeks, 7 days a week, 24 hours a day at 20 data points per hour for a total of 13,440 data points. In addition, each person taking part in the field test is assigned a dashboard to complete the digital survey on their personal computers. The field test participants were asked during the period of the field test to fill (at least) three times a day the digital survey. An IoT gateway establishes a local network, in which the thermal comfort stations and the digital survey are connected to the web server hosted in the portable main station. The locations of the thermal comfort stations in the office environment, as well as the portable main station and the IoT gateway are shown in Fig. 16. All participating offices have a similar size and the same orientation making the results comparable.

### 4.2. Results of the field test

During the field test, the building occupants voted 272 times during the four weeks of the field test. The cumulative number of votes per building occupant is shown in Fig. 17. In the following subsections, the capability of the system to assess personalized thermal comfort is demonstrated.

#### 4.2.1. Environmental and personal parameters

Table 4 shows the weekly average of the environmental parameters collected by the thermal comfort stations and the two personal parameters obtained via the digital survey. The table also shows the basic

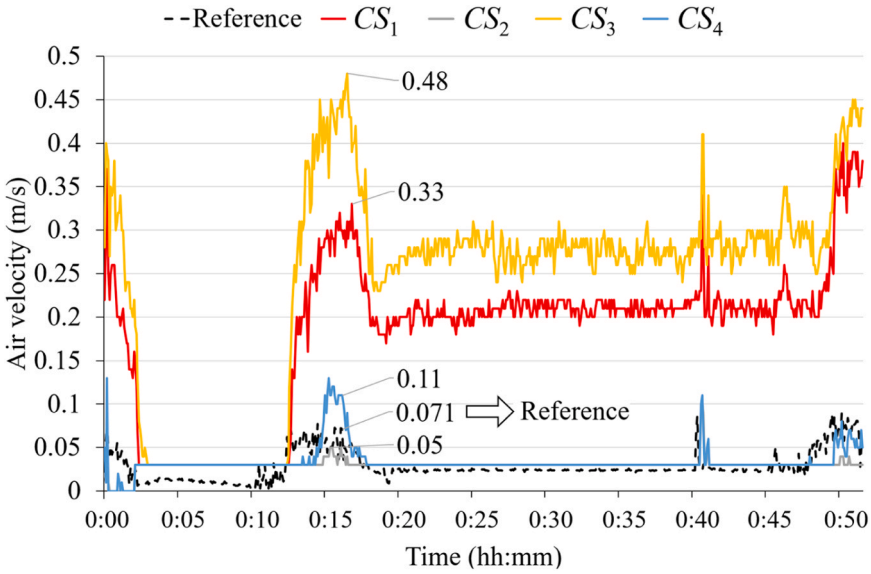


**Fig. 15.** Testing of the low-cost air velocity sensors before calibration.

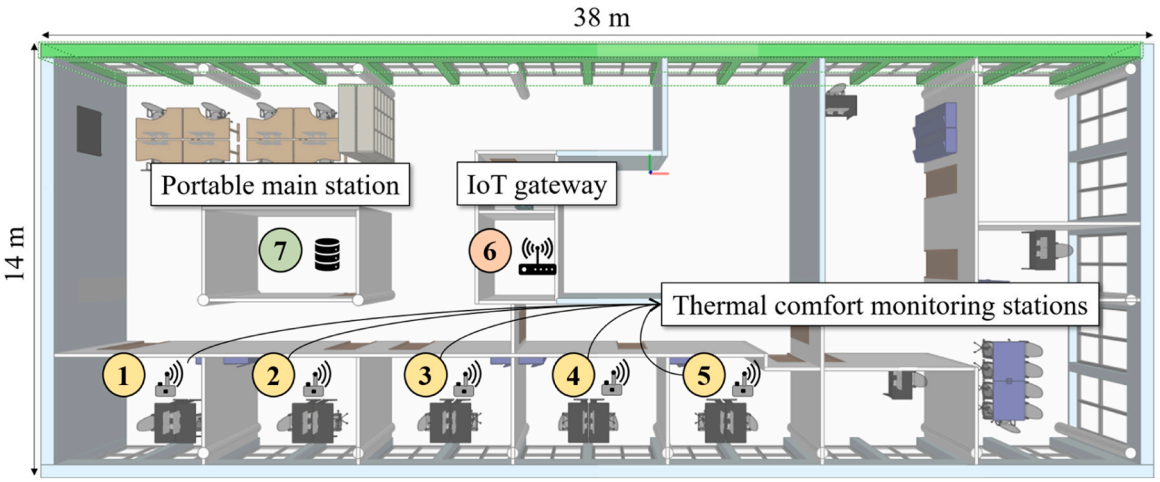


**Fig. 16.** Setup of the field test including the thermal comfort stations (1−5), the IoT gateway (6), and the portable main station (7).

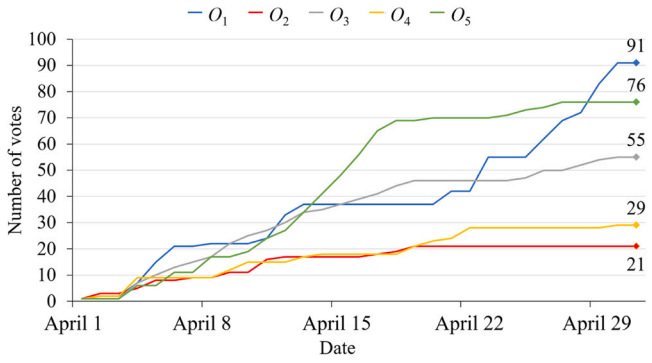


**Fig. 17.** Cumulative number of votes per building occupant (O - occupant).

**Table 4**
Weekly average values of the environmental and personal parameters.

| Week | $t_a$ (°C) | *RH* (%) | $v_a$ (m/s) | *MRT* (°C) | *Met* (met) | $I_{cl}$ (clo) |
|---|---|---|---|---|---|---|
| 1 | 26.24 | 24.63 | 0.12 | 26.06 | 1.10 | 1.00 |
| 2 | 26.81 | 22.76 | 0.11 | 26.50 | 1.18 | 1.01 |
| 3 | 27.22 | 28.20 | 0.10 | 26.82 | 1.17 | 0.87 |
| 4 | 27.60 | 34.67 | 0.16 | 27.19 | 1.19 | 0.60 |
| Average | 27.05 | 28.13 | 0.12 | 26.73 | 1.16 | 0.84 |
| Median | 27.16 | 26.57 | 0.12 | 26.67 | 1.14 | 1.01 |
| SD | 0.71 | 5.97 | 0.05 | 0.69 | 0.05 | 0.20 |
| Minimum | 25.48 | 22.00 | 0.03 | 25.69 | 1.08 | 0.57 |
| Maximum | 28.70 | 43.32 | 0.27 | 28.66 | 1.26 | 1.01 |

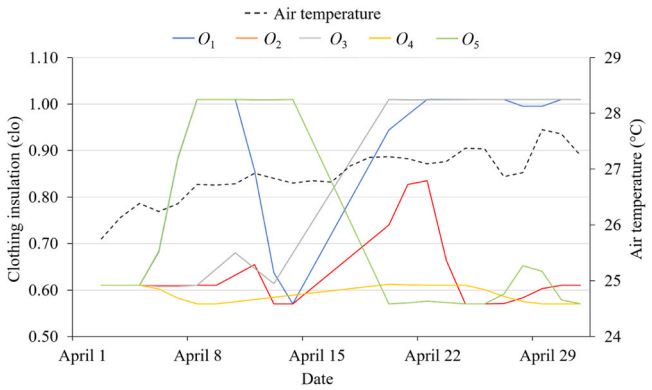


**Fig. 18.** Comparison of the clothing insulation values for all occupants.

descriptive statistics, including total average, median, and standard deviation (SD) as well as the minimum and maximum values, which can be used for further statistical analysis. As an example, the relation between clothing preference to the air temperature for all building occupants is presented (Fig. 18, Table 4). A correlation value of *corr* = - 0.66 is calculated from $t_a$ and the average $I_{cl}$ of all occupants indicating reduced clothing when the air temperature increases. However, individual differences can be observed in the results for each occupant. For example, ss observed from the figure, $O_1$ has constantly a larger clothing insulation value than $O_2$ for the same $t_a$, i.e. $O_1$ wears more clothes than $O_2$. The differences might be an indicator for the need of personalized thermal comfort.

### 4.2.2. *Subjective measures*

Table 5 summarizes the data collection results related to the subjective measures, including the basic descriptive statistics. The averages of the PMV index and the averages of the corresponding actual votes, both expressed on the 7-point scale, are summarized. In addition, the self-assessed productivity of the occupants is expressed on a five-point scale: Very unproductive (-2), unproductive (-1), normal (0), productive (1), and very productive (2). The thermal preference is expressed on a three-point scale: “I want it to be cooler” (-1), “no change” (0), and “I want it to be warmer” (1). On the one hand, the results show that in average, the building occupants self-assess the productivity between 0 and 1 for the conditions of the indoor environment. On the other hand, the results of the average thermal preferences show that the building occupants prefer to be cooler for weeks 1, 2, and 4, but would prefer a slightly warmer environment on week 2.

Fig. 19 compares the average PMV index and the average actual vote of all building occupants during the field test. The actual vote corresponds to the vote on the subjective thermal sensation on the 7-point scale entered by the building occupants via the digital survey. The personalized PMV index, also expressed in the 7-point scale, is

**Table 5**
Weekly average values of the subjective measures.

| Week | PMV | Actual vote | Productivity | Thermal preference |
|---|---|---|---|---|
| 1 | 0.69 | 1.86 | 0.04 | −0.92 |
| 2 | 0.92 | −0.26 | 0.24 | 0.13 |
| 3 | 0.89 | 0.18 | 0.01 | −0.02 |
| 4 | 0.68 | −0.40 | 0.46 | −0.46 |
| Average | **0.83** | **0.33** | **0.11** | **−0.29** |
| Median | **0.84** | **0.24** | **0.00** | **−0.14** |
| SD | **0.22** | **0.97** | **0.45** | **0.46** |
| Minimum | **0.36** | **−1.10** | **−1.00** | **−1.00** |
| Maximum | **1.13** | **2.00** | **1.00** | **0.62** |

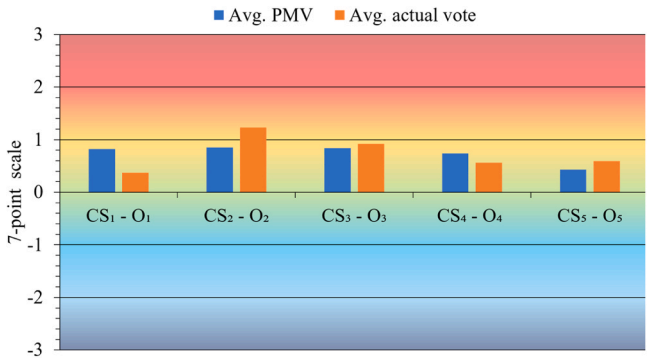


**Fig. 19.** Comparison of the personalized PMV index and the actual vote for all building occupants.

calculated by the thermal comfort stations and averaged over two weeks. The low-cost thermal comfort monitoring system aggregates and integrates the personalized PMV index and the actual vote, facilitating the comparison of the two values. By comparing the two average values, the suitability of the personalized PMV index to assess thermal comfort is examined. It is to be noted, that the analysis presented in this subsection showcases an example on how the system can be used to analyze thermal comfort data, in this case, by comparing the PMV index and the "actual vote". In the two-week data collection period, the absolute difference between the PMV index and the actual vote, depicted in Fig. 19 for all building occupants, are $O_1 = 0.45$, $O_2 = -0.38$, $O_3 = -0.08$, $O_4 = 0.18$ and $O_5 = -0.16$, respectively, indicating that thermal comfort is perceived uniquely by each occupant. However, the applicability of the PMV index for personalized thermal comfort is limited and other methods have been proposed [59]. The applicability of the PMV index and the limitations, are discussed in Section 4.3.

#### 4.2.3. Interactions with the built environment

In addition to studying the suitability for thermal comfort monitoring, the interaction of the building occupants with the built environment can be studied by considering the use of fans, the state of the windows and shades, as well as the use of lights in the offices. Exemplarily, Fig. 20 shows the air temperatures measured by the comfort stations ($CS_1$ to $CS_5$) over a regular working day. For example, by opening the windows in the room monitored by $CS_4$, the $t_a$ drops, as can be seen from Fig. 20. After closing the windows, the temperature increases again. Similar drops in temperature due to window openings can be observed in the figure for all $CS_n$. Through the digital survey, the occupants provide the thermal comfort monitoring system with the moments when the windows are open. Thus, the system is able to collect both the temperature drops and the moments when the windows are open, laying the foundations for future work, in which the data will be

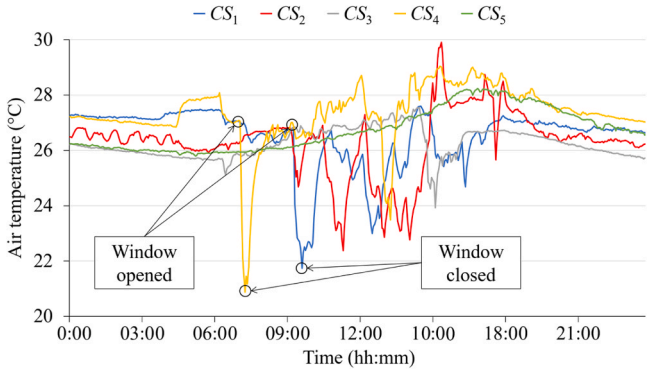


**Fig. 20.** Changes in air temperature when windows are opened and closed on one working day.

used for training artificial intelligence models to automatically detect the state of windows.

### 4.3. Discussion of the results

The validation tests have been conducted to evaluate the capability of thermal comfort monitoring system to personalize thermal comfort assessments. This subsection presents an analysis of the results obtained from the field test, highlighting the advantages and limitations of the study. In summary, the main advantages of the low-cost thermal comfort monitoring system are the following:

- *Low-cost hardware components*: By being budget-friendly, and competing in price with other low-cost comfort monitoring systems, the personalized thermal comfort monitoring system is accessible to a wider range of users, including smaller organizations, research projects with limited funding, and individuals. Using low-cost sensors and a low-cost microcontroller facilitates the scalability of the system, making it more feasible to deploy a larger number of sensors across a facility or multiple locations. Scaling the system allows for comprehensive coverage, enabling a more detailed and accurate assessment of thermal conditions in different areas.
- *Free and open-source software*: The software embedded into the thermal comfort stations is developed with open-source tools and, due to its modularity, can be extended and re-used for other implementation cases. Moreover, the web server is based on the Node-RED framework, which is free, open source, and compatible with common operating systems, including the Raspbian operating system used in this project, allowing for connecting to widely used cloud database services, such as InfluxDB or MongoDB, or for integrating data from external sources, such as weather forecast websites.
- *Personalization*: The monitoring system enables personalized thermal comfort assessment by collecting individual preferences and responses through digital surveys, seamlessly integrated with environmental data. The data can be utilized for tailoring the built environment to meet specific occupant needs and for optimizing comfort and energy efficiency. In Subsection 4.2.2, the discrepancies between the PMV index and the actual vote may occur, for example, if the air temperature is high but the occupant feels cold. It is true that the limitations of the PMV model are well documented in the literature [59]. While improved variations, such as the new predicted mean vote (nPMV), the extended predicted mean vote (ePMV), and the adaptive predicted mean vote (aPMV), demonstrate better predictions of actual votes, they all share the same major limitation, which is providing a "mean" vote for the "average" user, which does not reflect the complexity of individual adaptation and thermal comfort preferences in rooms occupied by multiple users. The system proposed in this study aims to calculate PMV and simultaneously collect the actual votes of the users, with the goal of creating a thermal comfort profile and a personalized PMV for each user in the future. Thus, each occupant will have a different adaptation coefficient, which is derived and developed over time as users continue to provide actual votes. The standard PMV has been used as the basis for this personalization process (instead of, e.g., aPMV) because of its acceptability as a standardized model adopted by thermal comfort standards, such as ISO 7730 and ASHRAE 55.
- *Automation*: The monitoring system, being IoT enabled, allows for automating data collection and analysis. By connecting actuators, such as humidifiers, automatic window controls or smart heating and cooling devices, the system also allows controlling environmental conditions. The automation through IoT technology reduces the manual workload, ensures real-time monitoring, and facilitates timely adjustments of control systems based on thermal comfort data, which reduces energy consumptions in buildings. Thermal preferences of building occupants can be used to implement control strategies to optimize thermal comfort using HVAC systems and

personalized comfort systems while reducing the energy consumption in buildings. Control strategies based on PID controllers, fuzzy logic, particle swarm optimization, multi-agent systems, and reinforcement learning may be implemented using the thermal comfort sensation obtained with through the survey.

- *Ease of use*: Leveraging IoT technologies streamlines the process of both data collection and user interaction. Digital surveys can easily be distributed and completed with reduced occupant effort, while sensor nodes can be deployed in a *plug-and-play* style in different locations of an indoor environment, thanks to the wireless communication inherent to IoT devices. The incorporation of IoT technologies in collecting occupant feedback may contribute to an improved overall participation of occupants in the survey process, aligning with current research interests.

While highlighting the several advantages as mentioned above, it is important to acknowledge that further work is needed to enhance the personalization and automation of the monitoring station. The following list discusses possible future efforts.

- *Calibration of the PMV value using the thermal comfort stations:* A calibration that explains the uncertainties and errors of the whole thermal comfort station should have been tested with the reference sensors in separate experiments after all sensors had been calibrated. If the PMV index calculated by the thermal comfort station wants to be sued reliable, static and dynamic experiments should be conducted in the climate chamber at different temperatures. For the dynamic experiments, it is also to be noted that the response times of reference sensors may be larger, such as in the case of the reference globe thermometer, in which the response time is 15 min.
- *Machine learning (ML) for thermal comfort personalization*: While ML models for personalization are not implemented in the system, the database built over time opens opportunities for future ML integration, particularly to address seasonality patterns and further enhance personalization through prognostics. ML models may be included into the web server. Moreover, libraries are available for implementing ML applications that are supported by low-cost and low-power microcontrollers, such as the ESP32 used in this study. By implementing ML applications onboard microcontrollers of the sensor nodes, the low-cost thermal comfort monitoring system may be further automated and decentralized.
- *Integrating actuator components*: Although actuators for automating HVAC systems or automatically opening and closing windows and shades are available, actuator technology is not widely deployed or is expensive due to specific hardware components and software licenses. In the current study, actuators are not yet included; rather, the thermal comfort monitoring system serves as a reliably basis to provide recommendations to building occupants to manually interact with the environment, by integrating actuators and personalized comfort systems to the system developed in this study.
- *Occupant data collection*: The dependence on building occupants for data collection presents limitations, as occupants must access digital surveys, and no specific strategies have been implemented to ensure regular participation. Future research may explore innovative methods to automate data collection, potentially leveraging ML to analyze the data for insights into occupant behaviors. In addition, window usage, lighting conditions, or personal parameters may be identified through computer vision techniques. For example, a webcam or mobile robot equipped with a stereo camera and computer vision algorithms could detect the presence of building occupants and identify the activity of the occupants to determine metabolic rate values.
- *Addition of further sensors*: Furthermore, it is recommended to focus on further aspects related to the environmental data to be collected by the thermal comfort stations and the feedback obtained from the occupants through digital surveys. Therefore, further sensors may be added to account for further measurements, such as $CO_2$. Adding lights sensors and sensors to detect the state of a window (open or closed) may be added as well to automate the collection of data related to the state of building elements, which is currently conducted through the digital survey. Moreover, the limitations of the accuracy of the low-cost air velocity sensor have been highlighted during the calibration process. Thus, the thermal comfort stations may include new air velocity sensors when a good alternative is available on the market.

## 5. Summary and conclusions

This paper has presented a low-cost thermal comfort monitoring system, which is characterized by a four-layer IoT architecture, low-cost hardware components, and embedded software applications. The system aims at automating data collection and integration to enhance the accuracy of thermal comfort assessments and reducing errors known from paper-based surveys, caused by manual integration and processing of data. The low-cost thermal comfort monitoring system, including thermal comfort stations, a portable main station based on RPi, and a digital thermal comfort survey, successfully collected personalized thermal comfort data during a long period of time. The collection of data is maximized thanks to the continuous measurement of environmental parameters by the thermal comfort stations, each built for less than 50 €. The effort of building occupants to give feedback on (i) personal parameters, i.e. clothing insulation and activity levels, (ii) subjective measures, i.e. actual votes, thermal preferences, and productivity, and (iii) interactions with the built environment, i.e. windows, fans, shades, and lights, is reduced by developing a web application that includes a personal digital survey. The digital survey improves the collection of occupant feedback that is often conducted manually with paper-based surveys, and integrates the feedback with the environmental data collected by the thermal comfort stations, facilitating posterior data analysis. Thus, the innovation of this work focuses on developing a low-cost and open-source personalized thermal comfort monitoring system, capable of autonomously integrating environmental data with feedback from building occupants, who can fill a digital survey designed to collect personal parameters, subjective measures, and interaction with the building with minimal effort for the occupant.

To obtain the maximum accuracy of the data collected by the thermal comfort stations, each low-cost sensor has been calibrated in several experiments under controlled conditions, which is another main aspect of this work. The calibration experiments are conducted in a climate chamber using high-precision reference sensors. After calibrating the sensors, a field test has been conducted to validate the capability of the low-cost thermal comfort monitoring system to personalize thermal comfort assessments. Personalized thermal comfort is assessed by statistically investigating the environmental parameters collected by the thermal comfort stations and the feedback obtained from the building occupants via the digital thermal comfort survey. The results of the field test show that the low-cost thermal comfort monitoring system can continuously and reliably collect thermal comfort data over long periods of time.

This paper contributes to research in the field of thermal comfort by providing a system that facilitates investigating personal parameters, preferences, and productivity of building occupants, as well as the interaction between occupants and the built environment. Furthermore, the system is capable of personalizing thermal comfort models, such as the PMV model, to examine the suitability by comparing the results of the models with feedback on thermal sensation or thermal preferences of building occupants. In future research, based on the recommendations summarized in Section 4, the low-cost thermal comfort monitoring system may be used in large-scale thermal comfort surveys, or to control personalized comfort systems via actuators. Besides incorporating actuators, cyber-physical and multi-agent systems consisting of autonomous software entities known from distributed artificial intelligence

may be used to link autonomous software agents with physical sensors and actuators to form a distributed monitoring system. Autonomous agents embedded into sensor and actuator nodes may coordinate, collaborate, and negotiate to perform tasks, such as maximizing thermal comfort by using actual votes to personalize the PMV index, minimizing energy consumption in buildings, or sending alerts to building occupants when the conditions of the environment are not satisfactory. Thus, in future studies, control and optimization algorithms will be investigated and implemented into the personalized thermal comfort monitoring system to enhance the ability to maximize thermal comfort while minimizing energy consumption of HVAC systems or personal comfort systems.

## CRediT authorship contribution statement

**Carlos Chillón Geck:** Writing – original draft, Validation, Software, Project administration, Methodology, Investigation, Formal analysis, Data curation, Conceptualization. **Kay Smarsly:** Writing – review & editing, Supervision, Resources, Project administration, Funding acquisition. **Conrad Voelker:** Writing – review & editing, Supervision, Resources, Project administration, Funding acquisition. **Hayder Alsaad:** Writing – review & editing, Validation, Resources, Methodology, Investigation.

## Declaration of Competing Interest

The authors declare that they have no known competing financial interests or personal relationships that could have appeared to influence the work reported in this paper.

## References


[1] A. Zivelonghi, M. Lai, Mitigating aerosol infection risk in school buildings: the role of natural ventilation, volume, occupancy and CO2 monitoring, Build. Environ. 204 (29) (2021) 108139, https://doi.org/10.1016/j.buildenv.2021.108139.

[2] United Nations Environment Programme, "2021 Global status report for buildings and construction: Towards a zero-emission, efficient and resilient buildings and construction sector," Nairobi, Kenia, 2021.

[3] M. Fan, et al., A review of different ventilation modes on thermal comfort, air quality and virus spread control, Build. Environ., 212(3) (2022) 108831, https://doi.org/10.1016/j.buildenv.2022.108831.

[4] M.J. Mendell, A.G. Mirer, Indoor thermal factors and symptoms in office workers: findings from the US EPA BASE study, Indoor Air 19 (4) (2009) 291–302, https://doi.org/10.1111/j.1600-0668.2009.00592.x.

[5] J. Nriagu, "Encyclopedia of environmental health", 2nd ed., vol. 6, Elsevier, Amsterdam, Netherlands, 2019.

[6] S. Roaf, D. Crichton, F. Nicol. Adapting buildings and cities for climate change: a 21st century survival guide, Second ed., Elsevier, Amsterdam, 2009.

[7] A.M. Bueno, A.A. de Paula Xavier, E.E. Broday, Evaluating the connection between thermal comfort and productivity in buildings: a systematic literature review, Buildings 11 (6) (2021) 244, https://doi.org/10.3390/buildings11060244.

[8] C.-E.A. Winslow, L.P. Herrington, A.P. Gagge, Relations between atmospheric conditions, physiological reactions and sensations of pleasantness, Am. J. Epidemiol. 26 (1) (1937) 103–115, https://doi.org/10.1093/oxfordjournals.aje.a118325.

[9] P.O. Fanger, Thermal comfort. Analysis and applications in environmental engineering, 164-164, Therm. Comf. Anal. Appl. Environ. Eng. 92 (3) (1972), https://doi.org/10.1177/146642407209200337.

[10] J.Van Hoof, Forty years of Fanger's model of thermal comfort: comfort for all? Indoor Air 18 (3) (2008) 182–201, https://doi.org/10.1111/j.1600-0668.2007.00516.x.

[11] V. Tomat, A.P. Ramallo-González, A.F. Skarmeta Gómez, A comprehensive survey about thermal comfort under the IoT paradigm: is crowdsensing the new horizon? Sensors 20 (16) (2020) 4647, https://doi.org/10.3390/s20164647.

[12] E.M. Mthunzi, H. Alsaad, C. Voelker, K. Smarsly, An ultra-low-cost thermal comfort monitoring station, in: Bauphysiktage, Weimar, Germany, Sep. 2019.

[13] J.J. Peralta Abadía, C. Walther, A. Osman, K. Smarsly, A systematic survey of Internet of Things frameworks for smart city applications, Sustain. Cities Soc. 83 (1) (2022) 103949, https://doi.org/10.1016/j.scs.2022.103949.

[14] M. Kimmling, S. Hoffmann, Behaglichkeitsmonitoring – flächendeckend und kostengünstig mit der Sensorstation CoMoS, Bauphysik 41 (2) (2019) 111–119, https://doi.org/10.1002/bapi.201800037.

[15] F. Salamone, L. Belussi, L. Danza, M. Ghellere, I. Meroni, Design and development of nEMoS, an all-in-one, low-cost, web-connected and 3D-printed device for environmental analysis, Sensors 15 (6) (2015) 13012–13027, https://doi.org/10.3390/s150613012.

[16] T. Parkinson, A. Parkinson, R. de Dear, Continuous IEQ monitoring system: Context and development, Build. Environ. 149 (2019) 15–25, https://doi.org/10.1016/j.buildenv.2018.12.010.

[17] I. Demanega, I. Mujan, B.C. Singer, A.S. Anđelković, F. Babich, D. Licina, Performance assessment of low-cost environmental monitors and single sensors under variable indoor air quality and thermal conditions, Build. Environ. 187 (2021) 107415, https://doi.org/10.1016/j.buildenv.2020.107415.

[18] T. Kramer, V. Garcia-Hansen, O. Sara, climateBOX: A low-cost and open-source monitoring device for personal thermal comfort evaluation, Energy and Buildings 283 (2023) 112830, https://doi.org/10.1016/j.enbuild.2023.112830.

[19] F. Nicol, S. Roaf, Post-occupancy evaluation and field studies of thermal comfort, Build. Res. Inf. 33 (4) (2005) 338–346, https://doi.org/10.1080/09613210500161885.

[20] K. Smarsly and Y. Petryna, "A decentralized approach towards autonomous fault detection in wireless structural health monitoring systems," in: *7th European Workshop on Structural Health Monitoring*, Nantes, France, Jul. 2014.

[21] A. Sanguinetti, M. Pritoni, K. Salmon, A. Meier, J. Morejohn, Upscaling participatory thermal sensing: lessons from an interdisciplinary case study at University of California for improving campus efficiency and comfort, Energy Res. Soc. Sci. 32 (2017) 44–54, https://doi.org/10.1016/j.erss.2017.05.026.

[22] H. Metzmacher, M. Syndicus, A. Warthmann, J. Frisch, C. van Treeck, Modular personalized climatization testing infrastructure with smartphone-based user feedback, Build. Serv. Eng. Res. Technol. 44 (1) (2023) 91–105, https://doi.org/10.1177/01436244221132688.

[23] L.T. Graham, T. Parkinson, S. Schiavon, Lessons learned from 20 years of CBE's occupant surveys, Build. Cities 2 (1) (2021) 164–184, https://doi.org/10.5334/bc.76.

[24] C. Helbig, M. Ueberham, A.M. Becker, H. Marquart, U. Schlink, Wearable sensors for human environmental exposure in urban settings, Curr. Pollut. Rep. 7 (2021) 417–433, https://doi.org/10.1007/s40726-021-00186-4.

[25] E. Laftchiev and D. Nikovski, "An IoT system to estimate personal thermal comfort," in: 2016 *IEEE 3rd World Forum on Internet of Things (WF-IoT)*, Reston, VA, USA, Dec. 2016, pp. 672-677, doi: 10.1109/WF-IoT.2016.7845401.

[26] P. Jayathissa, M. Quintana, M. Abdelrahman, C. Miller, Humans-as-a-sensor for buildings—intensive longitudinal indoor comfort models, Buildings 10 (10) (2020) 174, https://doi.org/10.3390/buildings10100174.

[27] D. Sheikh Khan, J. Kolarik, P. Weitzmann, Occupants' interaction with an occupant voting system for thermal and indoor air quality feedback – Case studies in office spaces, Front. Built Environ. 7 (2021) 643630, https://doi.org/10.3389/fbuil.2021.643630.

[28] J.R. Molina, V.L. Nakama, G. Lefebvre, A low-cost measurement device for recording perceptions of thermal comfort, J. Phys. Conf. Ser. 1433 (2020) 012006, https://doi.org/10.1088/1742-6596/1433/1/012006.

[29] W. Torresani, N. Battisti, A. Maglione, D. Brunelli, and D. Macii, "A multi-sensor wireless solution for indoor thermal comfort monitoring," in: *2013 IEEE Workshop on Environmental Energy and Structural Monitoring Systems*, Trento, Italy, Sep. 2013, pp. 1-6, doi: 10.1109/EESMS.2013.6661697.

[30] M. Sulzer, A. Christen, A. Matzarakis, A low-cost sensor network for real-time thermal stress monitoring and communication in occupational contexts, Sensors 22 (5) (2022) 1828, https://doi.org/10.3390/s22051828.

[31] B. Yang, M. Wu, Z. Li, H. Yao, F. Wang, Thermal comfort and energy savings of personal comfort systems in low temperature office: a field study, Energy Build. 270 (2022) 112276, https://doi.org/10.1016/j.enbuild.2022.112276.

[32] W. Jung, F. Jazizadeh, Human-in-the-loop HVAC operations: a quantitative review on occupancy, comfort, and energy-efficiency dimensions, Appl. Energy 239 (3) (2019) 1471–1508, https://doi.org/10.1016/j.apenergy.2019.01.070.

[33] K. Boudier, S. Hoffmann, Analysis of the potential of decentralized heating and cooling systems to improve thermal comfort and reduce energy consumption through an adaptive building controller, Energies 15 (3) (2022) 1100, https://doi.org/10.3390/en15031100.

[34] H. Alsaad, C. Voelker, Could the ductless personalized ventilation be an alternative to the regular ducted personalized ventilation? Indoor Air 31 (1) (2021) 99–111, https://doi.org/10.1111/ina.12720.

[35] H. Alsaad, C. Voelker, Performance evaluation of ductless personalized ventilation in comparison with desk fans using numerical simulations, Indoor Air 30 (4) (2020) 776–789, https://doi.org/10.1111/ina.12672.

[36] A.H. Osman, M. Artus, H. Alsaad, C. Koch, C. Voelker, Assessing a thermoelectric radiative cooling partition as a personalised comfort system using empirical experiments enhanced by digital shadow visualisation, Build. Environ. 245 (2023) 110833, https://doi.org/10.1016/j.buildenv.2023.110833.

[37] M.W. Ahmad, M. Mourshed, B. Yuce, Y. Rezgui, Computational intelligence techniques for HVAC systems: a review, Build. Simul. 9 (2016) 359–398, https://doi.org/10.1007/s12273-016-0285-4.

[38] D. Weinberg, Q. Wang, T.O. Timoudas, C. Fischione, A review of reinforcement learning for controlling build-ing energy systems from a computer science perspective, Sustain. Cities Soc. vol. 89 (9) (2023) 104351, https://doi.org/10.1016/j.scs.2022.104351.

[39] J.J. Peralta Abadía and K. Smarsly, "Internet of Things Frameworks for Smart City Applications—A Systematic Review," in: *ASCE International Conference Computing in Civil Engineering 2021* , Orlando, FL, USA, May 2022, doi: 10.1061/9780784483893.011.

[40] D. Legatiuk and K. Smarsly, "An abstract approach towards modeling intelligent structural systems," in: *9th European Workshop on Structural Health Monitoring*, Manchester, UK, Jul. 2018. e-Journal of Nondestructive Testing Vol. 23(11). ⟨https://www.ndt.net/?id=23207⟩.

[41] K. Dragos and K. Smarsly, "Decentralized infrastructure health monitoring using embedded computing in wireless sensor networks," in: *Dynamic Response of Infrastructure to Environmentally Induced Loads*, vol. 2, A.G. Sextos and G.D. Manolis, Eds., Lecture Notes in Civil Engineering, vol. 2., Cham, Switzerland: Springer International Publishing AG, 2017, pp. 183-201. doi: 10.1007/978-3-319-56136-3_10.

[42] K. Dragos, K. Smarsly, A hybrid system identification methodology for wireless structural health monitoring systems based on dynamic substructuring, in: Sensors and Smart Structures Technologies for Civil, Mechanical, and Aerospace Systems 2016, SPIE, Las Vegas, NV, USA, Mar. 2016, pp. 969–980, https://doi.org/10.1117/12.2219054.

[43] OpenJS Foundation, "Node-RED." Accessed: Jun. 15, 2022. [Online]. Available: ⟨https://nodered.org⟩.

[44] SiliconLabs, "Si7021-A20 Datasheet." Accessed: 15. 06, 2024. [Online]. Available: ⟨https://cdn-learn.adafruit.com/assets/assets/000/035/931/original/Support_Documents_TechnicalDocs_Si7021-A20.pdf⟩.

[45] Modern Deviceind Sensor Rev. C.," Modern Device. Accessed: Oct. 04, 2023. [Online]. Available: ⟨https://moderndevice.com/products/wind-sensor⟩.

[46] B&B Sensors, "Datasheet TSIC206." Accessed: Oct. 04, 2023 [Online]. Available: ⟨https://b2c.bb-sensors.com/out/media/Dat%20sheet_Digital_temperature_sensor_TSIC206_306.pdf⟩.

[47] Espressif Systems, "ESP32 Series Datasheet." Accessed: Jun. 15, 2022. [Online]. Available: ⟨https://www.espressif.com/sites/default/files/documentation/esp32_datasheet_en.pdf⟩.

[48] JST, "PH Connector, disconnectable crimp style." Accessed: Oct. 04, 2023 [Online]. Available: ⟨https://cdn-reichelt.de/documents/datenblatt/C100/JST_PHXP_BU_DB_EN.pdf⟩.

[49] JST, "EH Connector, Disconnectable crimp style." Accessed: Oct. 04, 2023 [Online]. Available: ⟨https://www.jst-mfg.com/product/pdf/eng/eEH.pdf⟩.

[50] ASHRAE, "ASHRAE Standard 55-2020. Thermal Environmental Conditions for Human Occupancy," American Society of Heating, Refrigerating and Air-Conditioning Engineers, USA, 2020.

[51] ISO, "ISO: 7730: Ergonomics of the thermal environment - analytical determination and Interpretation of thermal comfort using calculation of the PMV and PPD indices and local thermal comfort criteria," International Organization for Standarization, Geneva, Switzerland, 2005.

[52] F. Nicol, M. Humphreys, S. Roaf. Adaptive thermal comfort: Principles and practice, First ed., Routledge, London, UK, 2012.

[53] Almemo, "AMR WinControl." Accessed: Oct. 04, 2023 [Online]. Available: ⟨https://www.atp-messtechnik.de/media/pdf/2b/e7/28/SW-5600-WC2_SW-5600-WC2_D_Datenblatt.pdf⟩.

[54] Ahlborn, "Ahlborn pt100 NTC temperature sensors." Accessed: Oct. 04, 2023 [Online]. Available: ⟨https://www.ahlborn.com/assets/uploads/general/Produkte/Sensoren/Pt100-Fuehler-und-NTC/Verschiedene-Bauformen.pdf⟩.

[55] Ahlborn, "Ahlborn humidity sensor." Accessed: Oct. 04, 2023 [Online]. Available: ⟨https://www.ahlborn.com/assets/uploads/general/Produkte/Sensoren/Digitaler-Fuehler-FHAD46-Cx/Digitaler-Fuehler-fuer-Luftfeuchte-FHAD46.pdf⟩.

[56] Ahlborn, "Globe thermometer." Accessed: Oct. 04, 2023 [Online]. Available: ⟨https://www.ahlborn.com/assets/uploads/general/Produkte/Sensoren/Raumklimamessung/Behaglichkeit.pdf⟩.

[57] Ahlborn, "Air velocity sensor FV A605 TA." Accessed: Oct. 04, 2023 [Online]. Available: ⟨https://www.atp-messtechnik.de/media/pdf/43/05/14/FV-A605-TA1OD_FV-A605-TA1OD_D_Datenblatt.pdf⟩.

[58] Ahlborn, "Digitales Thermoanemometer omnidirektional FVAD 05-TOKx," Deutsch. Accessed: Nov. 29, 2023. [Online]. Available: ⟨https://www.ahlborn.com/produkte/digitales-thermoanemometer-omnidirektional-fvad-05-tokx⟩.

[59] S. Miao, B. Gangolells, B. Tejedor, Improving the thermal comfort model for students in naturally ventilated schools: Insights from a holistic study in the Mediterranean climate, Build Environ 258 (2024) 111622, https://doi.org/10.1016/j.buildenv.2024.111622.